STRUCTURE AND ACTIVITY PREDICTIONS ON SUPPORTED MONO- AND BI-METALLIC CATALYSTS

A THESIS SUBMITTED TO
THE GRADUATE SCHOOL OF NATURAL AND APPLIED SCIENCES
OF
MIDDLE EAST TECHNICAL UNIVERSITY

BY

EBRU ERÜNAL

IN PARTIAL FULFILLMENT OF THE REQUIREMENTS
FOR
THE DEGREE OF MASTER OF SCIENCE
IN
CHEMICAL ENGINEERING

APRIL 2006

Approval of the Graduate School of Natural and Applied Sciences

_____

Prof. Dr. Canan Özgen
Director

I certify that this thesis satisfies all the requirements as a thesis for the degree of Master of Science.

_____

Prof. Dr. Nurcan Bac
Head of Department

This is to certify that we have read this thesis and that in our opinion it is fully adequate, in scope and quality, as a thesis for the degree of Master of Science.

_____	_____
Prof. Dr. Şinasi Ellialtıoğlu Co-Supervisor	Prof. Dr. Deniz Üner Supervisor

Examining Committee Members

Prof. Dr. Terry S. King (Kansas State University, Chem. Eng.)	_____
Prof. Dr. Deniz Üner (M.E.T.U., Chem. Eng.)	_____
Prof. Dr. Şinasi Ellialtıoğlu (M.E.T.U., Physics)	_____
Prof. Dr. Işık Önal (METU, Chem. Eng.)	_____
Assist. Prof. Dr. Ersen Mete (Balıkesir University, Physics)	_____

I hereby declare that all information in this document has been obtained and presented in accordance with academic rules and ethical conduct. I also declare that, as required by these rules and conduct, I have fully cited and referenced all material and results that are not original to this work.

Name, Last name : Ebru Erünal

Signature :

CHAPTER I

INTRODUCTION

Bimetallic catalysts have widespread use in industry for a number of reasons: first, the activities of the individual metals can be combined; second, synergistic effects can occur due to alloying; third, the alloys may produce unique surface compositions and structures with improved activities and selectivities. Also, it is rather common to use a second metal to improve the thermal stability or poison resistance of the existing catalyst. One of the best examples is the industrial use of Pt-Pd bimetallics in hydrogenation reactions because of their sulfur resistance [1].

Supported metal catalysts may assume a variety of sizes and shapes. Their size and shape depend on the surface free energies and the energy of interaction between the metal particles and the support surface. In Fig. 1.1, the most common structures observed in the supported metals and their nomenclature is presented. As can be seen from the Fig. 1.1, the surfaces of the catalysts are composed of planar surfaces of (100) and (111) and defect-like structures at the edges and cornes of the particles. These surfaces may posess different reactivities depending upon the nature of the reaction. When more than one metal is involved, the relative distribution of these metals on the surface of the clusters can determine the relative activity of the catalyst.

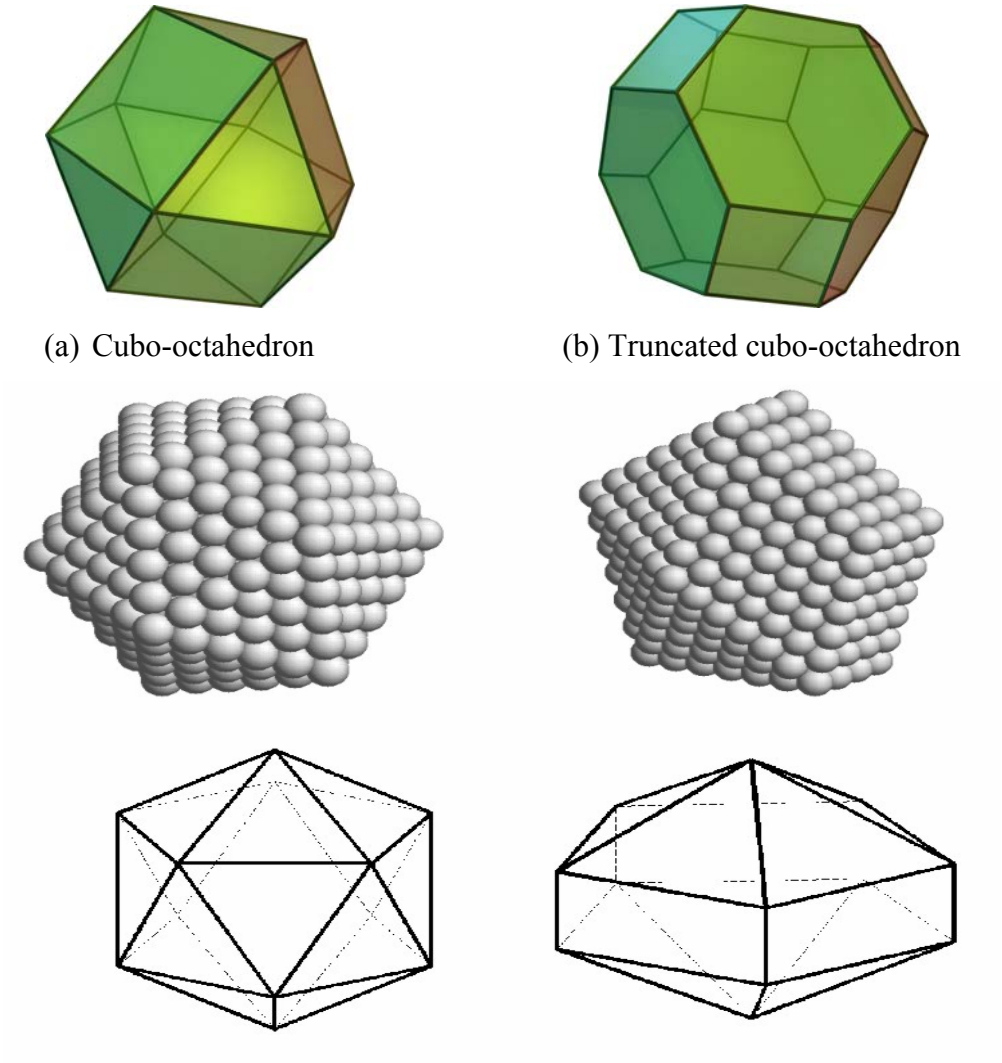

(a) Cubo-octahedron (b) Truncated cubo-octahedron

(c) Icosahedral (d) Decahedral

Figure 1.1 The most common structures observed in the supported metals [2,3,4]

Bimetallic catalysts may exhibit unique structure-activity relationships. At the beginning, the behavior of alloy catalysts was interpreted by both the electronic theory of catalysis and the Rigid Band Theory (RBT) of alloys [5]. The former theory stated that molecules are activated during the adsorption process by either releasing or accepting one electron, whilst the latter postulated that alloying a metal containing more valence electrons could decrease the number of *d*-band

holes via an electron transfer. Actually, the interpretation of the alloying effect has been found to be much more complicated later, though this initial concept remained still ever stimulating. The structure-activity relationships now are often explained on the basis of electronic and/or geometric effects [5]. However, geometric and electronic influences cannot often easily be separated as independent parameters. For instance, increasing the size of metallic particles results in an electron bandwidth increase and a decrease of binding energies of core electron, but the nature of the exposed planes and the topology of the surface sites change as well. There is the possibility, under high temperature conditions or very reactive atmospheres that surface mobility smoothes out geometric and structural features on small particles [5].

1.1 Electronic Effect in Catalysis by Alloys

The key point in this model lies in the interaction between the *d*-band orbitals of the surface sites with the molecular orbitals of reactants and products. The intermediate compound formed by one reactant at the surface must be stable enough to be formed but not too stable since it must decompose to yield the products [6]. This can be correlated with the heat of adsorption of reactants and products, governed by the electronic factors, which should be neither too strong nor too weak to give the optimum coverage for species competing at the surface, or for the products to desorb. The degree of electronic interaction between valence electrons of the two components in alloys depends on the enthalpy of formation ΔH_f , it will be low if ΔH_f is positive, but strong if ΔH_f is negative [5].

1.2 Geometric Effect

Generally some reactions need more than one surface atom to proceed. Moreover, a specific arrangement between these atoms can be required in order to generate the active site. This geometric model is generally named as “ensemble-size”

model. The basic idea in “ensemble-size” model is that the rate is a function of the probability to find an ensemble of n free and neighbor atoms on which the adsorption of the reactant(s), and the further transformations, can occur [5].

1.3. Mixed-site Effect

A mixed-site is an active site where both components of the alloys participate in the catalytic transformation. In some cases, such a site can show a higher catalytic activity than any of the pure metals, without real alteration of the individual electronic properties [5].

The first step of understanding catalytic activity in a certain reaction is the characterization of the surface of the catalyst particle. But, the surface characterization of bimetallic catalysts is very difficult because of inadequate measuring techniques. Structure sensitive reactions such as ethane hydrogenolysis can be used to explore the surface structure of the bimetallic catalysts [7]. Low-energy ion scattering (LEIS) seems to be the most sensitive method to study surface segregation as has been shown for various bimetallic alloys [8]. However, it is a very expensive technique. Besides, sputtering during LEIS may change the surface composition by preferential sputtering and radiation-enhanced segregation, and diffusion.

The diffuculties in analyzing the surface by physical techniques caused the development of indirect methods in which Monte Carlo simulations technique is the most preferable one [9].

The objective of this study is to generate a Monte Carlo code capable of predicting bulk and surface compositions of bimetallic clusters. First, Pt-IB (IB=Au, Ag, and Cu) bimetallic clusters were simulated at different atomic ratios and different temperatures ranging between 298–1000 K for cubo-octahedral

shaped and clusters containing 201, 586, 1289, and 2406 atoms via Monte Carlo method by using available thermodynamic data (such as free energy mixing, and pure component properties) and the mixing rules used in classical thermodynamics. The calculations were based on the model of King [9] which used interaction energies between two atoms, interchanging energies, and partial bond energies. In the second part of this work, the surface composition of Pt-Pd bimetallic catalysts as a function of temperature and cluster size were estimated in order to offer further insight to the catalyst activity for CO oxidation reaction.

CHAPTER II

LITERATURE SURVEY

2.1. Experimental Studies

Pt-Pd bimetallic catalysts have been used in (de)hydrogenation reactions [10,11] oxidation reactions [12], (dehydro)cyclization reactions [13], reduction of nitrate in the nylon production and the hydrogen peroxide production, and even they have been used in electrochemical studies [14]. Therefore, there are many experimental studies reported in the literature that show the improvement of the catalytic activity for several reactions and investigations over the properties of Pt-Pd catalysts.

Cho et al. [15] demonstrated that the structural change of Pt-Pd bimetallic particles over methane combustion reaction resulted in the removal hysteresis behavior, which was emanated from the reversible structural transformation of pure Pd catalysts, of catalytic activity along heating temperatures.

Persson et al. [5] investigated the influence of co-metals (Co, Rh, Ir, Ni, Pt, Cu, Ag, Au) on bimetallic palladium catalysts for methane combustion by TEM, EDS, PXRD, and temperature-programmed oxidation (TPO). They found that Pt-Pd catalyst was the most promising because of its high activity amongst others. From the PXRD patterns Pd was observed in the metallic form in Pt-Pd and Pd-Au catalysts. The effect of PdO decomposition is observed for all bimetallic catalysts, except for Pd-Cu which had a very low activity up to 700 ˚C. After this point, they observed that the methane conversion started to increase rapidly for Pd-Cu

catalyst. Furthermore, Pd-Ag catalyst did not show a clear dip at the PdO decomposition temperature, but the methane conversion remained at constant value during the decomposition. A similar behavior was seen for Pt-Pd, but the conversion started to rise at a lower temperature than the temperature of Pd-Ag. Besides, Pt-Pd was much more stable for temperatures below 675 °C, before the PdO decomposition. At temperatures above the PdO decomposition, the methane conversion decreased for this catalyst as well. Pt-Pd obtained low activity of methane conversion for the first two temperature steps, at 475 °C and 525 °C, respectively. As a result, all catalysts from this group achieved a stable activity except Pd-Cu which displayed a very poor conversion, and therefore they could not decide whether the activity was stable or not. In methane conversion with PdAg catalyst, they obtained the highest activity of the catalysts amongst the co-metals Ni and Pt although its activity was not as good as that of Pt-Pd. In Pt-Pd and PdAu, alloy formation was supported by the TEM analysis. Moreover, no co-metal was found on the alumina support except the ones close to the palladium. The activity of Pt-Pd was found to be lower than that of the monometallic Pd catalyst. The methane conversion increased, on the other hand, instead of decreasing with time. As a result three different cases were observed for the behavior of the co-metals:

(i) the co-metal reacts with the alumina support to form a spinel phase,
(ii) the co-metal forms separate particles, or
(iii) the co-metal alloys with Pd.

When both the stability and the level of activity for methane combustion are considered, Pt-Pd is considered the most promising of the catalysts tested in this study. Pd-Ag was also very stable, but it was slightly less active than Pt-Pd. Co-metals forming a spinel structure (PdCo and PdNi) did not improve the stability of the activity of palladium catalysts. However, the spinel structure appeared to improve the thermal stability of the support material. Co-metals forming separate

particles (Pd-Rh, Pd-Ir, Pd-Cu, and Pd-Ag) could improve the stability, depending on whether the co-metals were in close contact with Pd. Co-metals forming an alloy with Pd (Pt-Pd and Pd-Au) obtained stable activity.

Coq and Figueras [16] reviewed the effect of co-metal on the performance of Pd-based bimetallic catalysts. They concluded that there was no single interpretation to explain the effect of co-metal on the performance of Pd catalysts in selective hydrogenation of highly unsaturated aliphatic hydrocarbons, hydrogenation of aromatics or hydrodearomatisation, hydrogenation of nitrogen-containing compounds, reactions involving CO, and hydrodechlorination. They suggested that depending on the nature of both the co-metal and the reaction, the beneficial presence of a co-metal could be interpreted in terms of geometric effects, electronic effects and/or mixed sites. Moreover, in many cases, the promotion of catalytic properties would be directly related to the method of catalyst preparation, which affects the chemical states of both Pd and the co-metal as well as their spatial distribution.

Chung and Rhee [17] prepared dendrimer-encapsulated Pt-Pd bimetallic clusters with different metal compositions and investigated the activity in partial hydrogenation of 1,3-cyclooctadiene reaction. Here dendrimers were described, as highly branched macromolecules, generally known as spherical-shaped structures having interior void spaces with a high degree of symmetry. With this study Chung and Rhee showed that the catalytic activity of Pt-Pd is increased as the Pd/Pt ratio decreased.

Kaya [18] examined CO oxidation over γ-Al_2O_3 supported mono- and bimetallic Pt-Pd catalysts which were prepared by two different methods as sequential impregnation and co-impregnation methods at Pd:Pt atomic ratios: 1:3, 1:1, 3:1. He did the catalyst performance tests in a temperature range between 373 K and 523 K with a synthetic gas mixture containing CO, O_2, and N_2. He observed the

same catalytic behavior with Pd monometallic and Pd containing bimetallic catalysts, interpreting this as Pd segregation on the surface of the co-impregnated catalysts.

Du Plesis and Taglauer [19] studied the surface concentration modification of Pt_xPd_{1-x} alloys (x = 0.3, 0.5, and 0.7) under ion bombardment with noble gas ion sputtering and measured the surface composition by low-energy ion scattering spectroscopy (ISS) and Auger electron spectroscopy (AES). They observed that Pd was preferentially sputtered from the surface of the alloys.

In another study by Du Plesis et al. [20], they measured five palladium–platinum alloys of different compositions ranging from 10 to 90% by Argon ion bombardment. They also developed a model for surface segregation to fit the experimental data. They reported the values for the surface segregation energy (ΔG) and the radiation-enhanced diffusion coefficient (D) as 2000–8000 J/mol and 1.2–8.0×10^{-20} m^2/s, respectively.

Hansen et al. [21] measured surface concentration profile for the three low-index surfaces of Pt-Pd (1:1) random alloys at 500, 1000, and 1500 K by EXAFS technique. Their findings also indicated Pd segregation to the surface.

Rades et al. [22] tried to demonstrate the strong alloying effect between highly dispersed platinum and palladium and from this point they tried to determine the reason for the synergy of Pt-Pd catalysts that have resistance to sulfur and nitrogen. They compared the results of hydrogen chemisorption of a Pt-Pd system in NaY zeolite and ^{1}H NMR with the formation of these alloys. They stated that this strong alloying effect changes the electronic structure of the metal exposed at the particle surface. It was suggested that this effect is responsible for the increased resistance towards Lewis base poisons. Another important result they reported was that the Pt-Pd alloy is likely to be formed at all platinum

concentrations, but particularly at about 40% of platinum. One may assume that the metal–metal bonds are, therefore, strongest in an alloy with about 40% of platinum and suggested that chemisorption can be expected to the weakest for alloys with platinum content of 40%. At the nanoparticle scale, this corresponds to a higher stability of the particles and hence to a lower reactivity of the metal surface.

Oetelaar et al. [8] examined the surface segregation in Pt-Pd alloys and Pt-Pd bimetallic nanoclusters on alimuna and carbon supports by determining the metal surface composition of these systems with low-energy ion scattering (LEIS). They looked at adsorbate/adsorbate, cluster size, and metal support interactions in Pt-Pd clusters. They found that the Pd (under UHV) surface concentration increased with increasing temperature for both Pd- and Pt-rich cases until at about 700 °C which was attributed to thermodynamic equilibrium condition. During the hydrogen and oxygen treatments an enhanced Pd surface enrichment was observed and thermodynamic equilibrium was reached at 400–500 °C. The Pt-Pd alloys were found to have a different surface composition than very small Pt-Pd nanoclusters in bimetallic catalysts although they had the same bulk composition. Cluster size had a strong effect on surface composition. For highly dispersed Pt-Pd catalysts with a metal dispersion close to 1 -corresponding to an average cluster diameter about 1 nm or smaller- surface segregation was completely suppressed due to a limited supply of Pd atoms from the bulk to the surface of the nanoclusters. For Pt-Pd catalysts with a low metal dispersion of about 0.3 and 0.8, Pd surface segregation takes place to approximately the same extent as in the Pt-Pd bulk alloys. They also determined Q_{seg} according to the Langmuir–Mclean expression; by assuming that thermodynamic equilibrium was reached at about 700–800 °C, since no increase in Pd surface concentration was observed beyond this temperature range. Moreover, they reported that increasing the temperature caused a slight decrease in Pd surface concentration. Since hydrogen and oxygen treatments did not result in surface segregation in the supported catalysts with

very small Pt-Pd clusters but gave rise to surface segregation in the catalysts with larger Pt-Pd clusters to approximately the same extent as in the bulk alloys, they said that with respect to the alloys the effect of hydrogen and oxygen on surface segregation in Pt-Pd nanoclusters was not large. For the lower dispersed catalysts, a $Pd_{80}Pt_{20}/Al_2O_3$ and $Pd_{73}Pt_{27}/C$ catalyst with a metal dispersion of about 0.8 and 0.3, respectively, a cluster size effect on the surface composition could not be seen. Both Pd and Pt had a fairly strong interaction with an alumina support. They recorded that the interaction of Pd and Pt with the carbon support did not differ significantly to affect surface segregation. Finally, they concluded that the cluster size effect was the main reason for the differences in surface segregation in the Pt-Pd alloys and alumina- and carbon-supported catalysts.

Rousset et al. [23] also studied the surface concentrations of Pt-Pd bimetallics obtained by the focusing of an Nd:YAG laser onto rods of alloys. Low energy ion scattering showed that the surface of the obtained bimetallics is Pd enriched: the Pd concentration in the first atomic layer is found to be equal to 38 at.% for a $Pt_{83}Pd_{17}$ rod composition and 87 at.% for the $Pt_{35}Pd_{65}$.

Besides these experimental studies, bimetallic Pt-Pd catalysts have been also studied from a theoretical point of view. Before the literature on these is reviewed, a brief description of the broadly used theoretical methods will be summarized below.

2.2 Theoretical studies

Generally speaking, in the literature, there are three major techniques that deal with the surface and bulk simulations of these systems:

i) *Ab inito* Methods
ii) Semi-Empirical Methods

iii) Dynamical Simulation Methods (Molecular Dynamics)

2.2.1 *Ab inito* Methods

These methods are based on the quantum chemical approaches, mainly dealing with the approximate solution of the time-independent, non-relativistic Schrödinger equation which gives the total energy for a molecular system consisting of *m* atoms and *n* electrons. In principle, it is impossible to solve this equation, because of the large number of electrons that exist in a solid. Therefore, further approximations are essential. Since, the empirical values are not used in these techniques, the results are mathematically rigorous. The values of the fundamental constants and the atomic numbers of the atoms present are used. In addition to this, systems involving electronic transitions can be considered by *ab initio* techniques because of being capable of calculating transition states and excited states. The density functional theory (DFT), in which the electron density is considered as the variable for the calculations in the related equation, is one of the most popular approximations among *ab initio* methods. [24]

Løvvik [25] investigated the surface segregation in Pd based alloys of twelve different metals (Ag, Au, Cd, Cu, Fe, Mn, Ni, Pb, Pt, Rh, Ru, and Sn) by density-functional band-structure theories. He proposed that the segregation energy is an indirect measure of the stability of Pd based hydrogen permeable membranes. He examined both the geometric and electronic effects in order to explain the segregation. It was suggested that the segregation energy -which was defined as the difference in calculated uncorrected total free energy between a surface (or near surface) site and a bulk-like site- is correlated with both the difference in radius and the difference in surface energy between the two metals of the palladium based alloys of this study. There was a negative correlation between the segregation energy and the size of the substituted atoms (measured by their covalent radii) and a positive correlation between the segregation energy and the

experimental surface energy of the metals. Besides, he stated that the segregation of metal atoms at the grain surfaces was not necessarily the same as the segregation at surfaces towards vacuum, since impurities only located in the grain boundaries may bond more strongly to one of the metals of the alloy.

Neyman and Illas [26] made an overview about the studies dealing with density functional theories for heterogeneous catalysts, their adsorption properties and reactivities. They gathered results of cluster and slab model calculations and compared them with experimental results. Besides, they gave a brief review about problems and limitations of density functional applications.

2.2.2 Semi-Empirical Methods

These techniques use approximations to provide the input from empirical data into the mathematical models. Although, they are based on quantum physics and capable of calculating transition states and excited states as well, they are less computationally demanding than *ab initio* methods. However, they are not as rigiorus as *ab initio* methods. They can be used for medium-sized systems such as those having hundreds of atoms. [24]

Cox et al.'s research [27] was based on the surface properties of Pt and Pd using an empirical two- plus three-body potential developed for cubic elemental solids according to the study of Murrell and Mottram [28]. They derived the parameters of the potential by fitting phonon frequencies, elastic constants, vacancy formation energy, lattice spacing, and cohesive energy. They demonstrated that it was possible to reproduce surface phenomena just by fine-tunning the values of the two- and three-body parameters, without the use of surface properties in the fitting. They could reproduce the fcc structural data, the experimental energies and also the relaxation of the (111), (110), and (100) surfaces of fcc Pt and Pd to a high degree of accuracy.

In their study, Rousset, Bergolini, and Miegge [29] made a model based on the equivalent-medium approximation in order to calculate the energies of surface layers as a function of local concentration for determining the surface composition of several fcc Pd-based alloys. They also considered bond strength modifications at the surface that were determined within a modified tight-binding scheme. For Pt-Pd system, they recorded a nearly regular exothermic alloy with low heat of mixing and Pd enrichment on the surface layers was observed. Although they also observed a surface enrichment for Pd especially on the first layer, this enrichment seemed to be higher than the experimental findings [8].

Massen et al. [30] analysed the geometries and segregation profiles of platinum, palladium, and platinum-palladium clusters up to 56 atoms by many-body Gupta potentials which were calculated from the interatomic interactions. They obtained these Gupta potentials for Pt-Pd interactions by averaging those for Pt-Pt and Pd-Pd interactions. From global optimization studies, pure clusters of platinum and palladium were predicted to adopt a variety of structures, depending on the cluster size. Many of the structures were found to be regular (ordered), though there was a tendency (which was greater for Pt than for Pd) towards forming disordered structures. The predicted lowest energy structures for $(Pt\text{-}Pd)_M$ nanoalloy clusters have different geometric structures than the corresponding pure Pt or Pd clusters: with a reduced tendency to display icosahedral packing and a larger number of capped decahedral structures. (Some structures have already been given in Fig.1.1.) Besides, shell-like atomic segregation was found to be favoured for the Pt-Pd clusters, with the surface becoming richer in Pd and the core becoming richer in Pt. This segregation, which was consistent with experimental studies on PtPd particles, was explained in terms of the lower surface energy of Pd and the greater cohesive energy of Pt. For non-stoichiometric Pt-Pd clusters, the calculated global minimum was shown to depend strongly on the composition, with the doping of even a single Pt atom into a Pd cluster (or vice versa) being sufficient to change the geometrical structure of the cluster. They suggested that,

segregation was seen to be greatest for larger clusters experimentally may be because, as suggested by Gijzeman [31], the gain in energy on moving an atom from an internal to an external site is small in smaller clusters, where the internal sites are not truly bulk-like. Their results showed resemblence with Rousset et al.'s [32] experimental results in which they investigated alumina supported Pt-Pd catalysts with X-ray and TEM analysis. Both Massen [30] and Rousset [32] found a Pd rich surface shell while the core shell is rich in Pt. Another interesting finding of Rousset [32] is that the activities of the bimetallic catalysts for the vapor phase toluene hydrogenation did not show any synergy between Pd and Pt but rather a perfect additivity of their individual catalytic properties. Besides, Pt showed to have no electronic influence on the reactivity of Pd atoms.

2.2.3 Dynamical Simulation Methods (Molecular Dynamics)

The least intensive, fast, and useful -with limited computer resources- methods are molecular dynamics which use classical physics to explain and interpret the behavior of atoms and molecules. They are based on Newton's second law or the equation of motion. From knowledge of the force on each atom, the acceleration of each atom in the system is predicted. They require either *ab inito* or experimental data for calculating the parameters. However, they cannot calculate the electronic properties. They are best for the systems having neither breaking nor formation of bonds. They are appropriate for very large systems that contain thousands of atoms. Although, this method seems to be more advantageous amongst others, also longer running time and a much higher capacity computer is necessary [24].

2.2.4 Monte Carlo Method

Especially, for large molecular systems the computational complexity is enormous and supercomputers or specially attached processors are used to perform simulations spanning long enough periods of time. At this point, the question of

whether or not these techniques are better than experiments comes into minds as the time and the cost of the supercomputers considered. How can we obtain qualified data in shorter periods of time with simulation techniques? There is an alternative way to perform molecular simulations called Monte Carlo method based on exploring the energy surface by randomly probing the geometry of the molecular system. It is not only a practical method but also gives useful data in shorter time ranges and in contrast with the other techniques the performance of the computer need not be so high in order to use this method. It is essentially composed of the following steps: The most popular realization of the Monte Carlo method for molecular systems is the Metropolis algorithm [33]**:**

1. The initial coordinates of atoms X_0^N are specified (e.g., from molecular mechanics geometry optimization).
2. New set of coordinates X_a^N by changing the initial coordinates of an atom at random is generated.
3. The change of potential energy ΔV corresponding to this displacement is calculated.
4. If $\Delta V < 0$ the new coordinates are accepted and step 2 is repeated for another atom.
5. Otherwise (if $\Delta V > 0$), a random number R in the range [0,1] is selected and:

a. if $\exp(-\Delta V/kT) \geq R$ the new coordinates are accepted and step 2 is repeated,

b. if $\exp(-\Delta V/kT) < R$ the original coordinates are kept and step 2 is repeated.

In a pioneering study about the simulation of bimetallic surfaces, Donnely and King [34] performed a Monte Carlo simulation of Cu-Ni alloy surface as a function of bulk composition, surface crystallographic orientation, and temperature. They computed the configurational energies in a manner which accounted for the variation of atom–atom bond with coordination number. Their findings were in reasonable agreement with published experimental results.

Strohl and King [35] modeled supported Pt-IB (IB= Cu, Ag, Au), Ag-Ru, and Pt-Rh bimetallic catalysts with a Monte Carlo method which uses a coordination-dependent potential model. Systems were between the dispersion range of 30% to 60% having both cubo-ochedral shapes and irregular shapes. They recorded that generally IB segregated to the surface of the catalyst in Pt-IB systems and tend to the lowest coordinated site first. As the concentration of IB increased, the surface segregation was also increased. Amongst IB atoms Au was observed to be the most segregated to the surface. They also said that the degree of clustering of Pt atoms on the surface of the catalyst particles depends on which IB element is present as for Au-Pt system having to produce larger ensembles of surface Pt atoms than the Ag-Pt or Cu-Pt systems.

A combined study was done by Drchal et al. [36] who researched the surface segregation and the energetics of the surface region of metallic alloys Pd-Ag and Pt-Rh with *ab initio* electronic structure calculations using the equation of motion and they as well performed the surface concentration profile and its dependence on the temperature by using a Monte Carlo simulation. Firstly, the internal energy with its dependence on the configuration of the system was found by *ab initio* methods, and secondly, the thermodynamic properties of the system were studied by methods of statistical mechanics.

Khanra and Menon [37] did a Monte Carlo simulation in order to predict the chemisorption effect in order to study the segregation behavior for a Pd-Ag bimetallic cluster. Differently from other Monte Carlo simulations that deal with segregation in bimetallics, they also estimated the oxygen chemisorption pressure-dependent surface composition of these clusters.

Deng et al. [38] studied surface segregation of Pt-Pd alloy at 800 K for 30, 50, 60, and 70% of Pd by fraction with Monte Carlo simulations. They used analytical embedded-atom method for modelling the alloy which was simulated as cubo-

shaped computational cell composed of 512 atoms with eight layers for the bulk-like computational cell and 1344-atom surface cell having 21 layers with 64 atoms per layer. The parameters required for the model used were derived from the properties of metals like lattice constant, cohesive energy, monovacancy formation energy, and elastic constants. They found that the topmost surface of the cluster is strongly enriched with Pd while the amount of Pd segregation in the (111) face is significantly less than (100) face that has a more open structure. On the other hand, their studies showed that Pd depleted on the subsurface layer. In addition to this, a damped oscillation of Pt concentration in the whole composition range of the alloy was observed.

De Sarkar et al. [6] made a study about the segregation behavior of supported, clean, and gas-covered Pt-Pd nanoparticles as a function of the metal support interaction with MC simulations. All of the nanoparticles were assumed to have an fcc cubo-octahedral geometry since both the Pd and Pt metals have the fcc structure. They calculated the configuration energy due to three components as pair-bond energy, the metal–support interaction energy, and energy owing to chemisorption effects. Their findings were that the average surface composition of the particles remained uninfluenced by the strength of the metal–support interaction. Besides, the presence of adsorbates did not influence the role of metal support interaction on the surface composition.

The valence shell electronic configuration of Pd in atomic form is of $4d^{10}5s^{0}$ type; in metallic Pd, approximately 0.36 electrons of the *d*-shell are in the *s*-band. This leaves an equivalent number of holes in the *d*-band. The filling of the 4*d* shell on alloying can therefore arise either by a flow of charge from *s*-band of Pd or a charge transfer from a second component [5]. Also**,** Fuggle et al. [39] concluded in their study that (i) in alloys with electropositive elements the Pd *d*-band is filled and moved away from the Fermi level with narrowing of the *d*-band width; (ii) as the electronegativity difference between the elements is decreased there is a

greater overlap in the band energies of Pd and second metal; (iii) the filling of bands is largely due to changes in the hybridization of the Pd *d*-band, and the actual charge transfer of Pd *d* electrons is probably small.

In another study by Strohl and King [40], a multicomponent, multilayer model of surface segregation in alloy catalysts of Ag–Au, Cu–Ni, and Au–Ni binary systems and the Cu–Ni–Pt ternary system were studied. They used both regular and Margules solution models and used surface free energy data. Their model included multicomponent capability that meant the components may be different sizes and the ability to use virtually any mixing model. They recorded that in Au-Ni system the greater segregation of Au was better aggrement with the experimental results.

More recent studies include the studies of Wang et al. [41] and Deng et al. [38]. Wang et al. [41] investigated the surface structures of cubo-octohedral Pt-Mo nanoparticles at 600 K using the MC method and modified embedded atom potentials method. Deng et al. [38] studied the surface segregation of Pt-Pd alloys at 800 K with Monte Carlo simulations again by using analytic embedded-atom method for cubo-shaped computational cells.

By using experimental bulk mixing data, Zhu and DePristo [42] predicted the microstructures of bimetallic clusters with 201 atoms having a 50%–50% composition for a cubo-octahedral shape. They also neglected any size effect. They used to parametrize the developed bond order metal simulator (BOS-mixing) model which characterizes the variation of metal–metal bond strength with number and type of atomic neighbors. The variations with coordination for homogeneous systems were taken from a previous work [43] that used the experimental dimer binding energies, surface energies, and cohesive energies. The variation with type of neighbor was determined by fitting the experimental mixing energies as a function of composition for bulk bimetallic systems. They found that

three effects determine the microstructures: the difference of surface energies, mixing energy, and entropy. The difference of surface energy always causes segregation of the atoms with lower surface energy to the lower coordinated sites, most obviously leading to surface enrichment of the atoms with lower surface energy. The mixing energy effect depends upon the sign: for positive values atoms favor having neighbors of the same type, while for negative values atoms favor having neighbors of the other type. The entropy term always favors mixing of atoms of different types. The microstructure of a cluster results from competition among these three terms. Sometimes one term may be so much larger than the others as to dominate the microstructure and thus make the prediction of the microstructure rather simple. They recorded that at 0 K the element having higher surface energy and occupying fcc(111) site had an average of 2.4–2.7 surface neighbors of the other type for the alloys with positive mixing energy. However, for the alloys with negative mixing energy (Pt-Pd) the element had 6 unlike surface neighbors. At high temperatures, both kinds of systems tend to have an equal number of unlike surface neighbors, which was close to the random distribution. They also observed for every system, the mixing increased with increasing temperature, although the amount depent sensitively on the surface energy difference compared to $T\Delta S$ (entropy effect). Thus, the first element occupied 18% of surface sites if it has higher surface energy or 83% of surface sites (80% for Pt-Pd) if it has lower surface energy. They mentioned that since having insufficient knowledge about the mixing energy for Pt-Pd alloys, they could not evaluate the ordering or disordering of the alloy strucure for them.

Experimentally, Ramaswamy et al. [44] investigated the dependence of layer thickness on stress behaviors during growth of Pd/Pt multilayer films. They used an in-situ substrate curvature measurement. They chose Pd/Pt multilayers because of their small lattice mismatch. They reported that due to a high density of interfaces in a multilayer (compared to a single component film of the same overall thickness), stress producing mechanisms associated with coherency,

surface and interface stresses, and alloy formation are expected to be dominant. Therefore, the contributions of coherency and surface stress to the evolving of the force in the film per layer width, and its dependence on the thickness of the layer directly beneath were considered. The stress measurements were done according to be independent of thermal stresses during multilayer deposition since no temperture change occured. Stress behavior throughout the initial Pt growth relies on the thickness of the Pd layers. They found that the intrinsic stress behaviors of Pt layers in samples with thick and thin Pd layers are identical, and that the observed difference is entirely due to coherency stress. By this understanding of stress evolution they also tried to explain the behaviors of Cu/Pd and Cu/Pt multilayers.

Kuijers et al. [45] did AES measurements and used several segregation models to obtain the surface composition of Pt-Pd samples (powders and evaporated films) with different bulk compositions after equilibration at 400 °C for 16 h. They found a good agreement between theory and experiment, using a regular solution model with a variable parameter Ω to introduce the "nonregular behavior" of ΔH_{mix}, i.e., that the heat of mixing in the Pt-Pd system is dependent on the bulk composition.

CHAPTER III

THEORY

3.1. Surface Thermodynamics

It can be easily shown with even simple thermodynamic arguments that the surface composition of a multicomponent system may be very different from its bulk composition. This fact can be attributed to the differences in bonding between like and unlike components in the mixture and the absence of some bonds in the surface result in a composition in the surface region different from the bulk composition [9]. Thermodynamically, it can be said that the creation of a surface is always accompanied by a positive free energy change. In order to minimize this surface free energy, the surface will be enriched by the constituent which has the lowest surface free energy. These results, for many multicomponent systems, are in gross imbalance between the surface composition in the top-most layer and in the bulk**.** Here the surface free energy is defined as the increase of the total free energy of the system per unit increase of the surface area. For metals, the creation of more surface area requires the breaking of chemical bonds which are accompanied by charge redistribution of the electron gas. It is therefore necessary to develop thermodynamic models that provide prediction of surface composition of multicomponent systems as a function of bulk composition and as a function of temperature**.** In general, the most widely known theory for these predictions is the monolayer model in which only the top-most layer of the surface is treated as distinct from all other layers that are assumed to have the bulk composition. Then, an expression is written for the chemical potentials of the surface and bulk phases. Finally, these chemical potentials are equated to give an

expression for the surface composition. By this approach, the surface layer and the bulk can be treated as ideal or regular solutions**.** The other popular theory is called as the multi layer model in which the two-component crystal is treated as an infinite set of layers of atoms (or molecules). Each layer is treated as having a possibly different composition ratio. Then, an expression is written for the free energy of this system with the atom fractions of each layer inserted as variable parameters which are varied to obtain the minimum free energy for the whole system. Each of the layers can be treated as either regular or ideal solutions [46].

King [9] classified the chemical models for surface segregation in two general types:

i) Macroscopic thermodynamic models in which the perturbation of the bonding properties at the surface of a material relative to the bulk is contained in the property of surface tension.
ii) The bond breaking models which describe the perturbation of the bonding mechanism by using a detailed knowledge of the bond energies (or enthalpies) in the surface region and the number of bonds associated with each atom in the surface region.

3.1.1. Macroscopic Thermodynamic Approach

The macroscopic thermodynamic approach requires as input data the pure component surface tensions, the pure component molar areas, the variation of molar area with mixing, and a mixing model (e.g., ideal, regular, or some non-regular mixing model) while no detailed bond energy data are needed. Since the model is based upon the postulates of classical thermodynamics, only a macroscopic picture of the surface is available; that is, only a composition profile for continous surfaces can be obtained. However, the constituents can be of different sizes. Also, it is difficult to model chemisorption. Even though this

approach is not so obviously tied to a physical picture, it also yields useful insight. The first person to lay the theroretical groundwork for the prediction of the surface segregation was Gibbs, who used the postulates of classical thermodynamics to derive the Gibbs adsorption isotherm:

$$\Gamma_A = -(\partial\sigma/\partial\mu_A)_{T,P} \quad (1)$$

in which Γ_A represents the surface excess of the component A in an A–B binary, σ the surface tension, and μ_A the chemical potential of A. From this equation, it can be seen that if an increased amount of A tends to lower the surface tension of he solution, then component A should be found in excess within the surface region. In other words, if mixing effects are ignored, for a given mixture the component that has the lowest surface tension will be enriched in the surface region.

In binary alloys, it has been observed that pure-component surface tension and pure-component cohesive energies are fairly good indicators of which component will segregate to the surface [9]. The surface tension of the solid surfaces will, in general, depend on the crystallographic orientation. This coupled with the effect of crystallite size (that is, the influence of curvature on surface tension) further increases the difficulty of obtaining reliable surface tension data. For monatomic solids surface tension determination is more difficult, and the available experimental data are scarce and often determined only at one temperature [46]. Overbury et al. [46] found a relationship between surface tension and sublimation energy and suggested that at least for monatomic solids the surface tension may be estimated when direct experimental determination is difficult or lacking:

$$\sigma_{sm} = 0.16\,\Delta H_{sub} \quad (2)$$

King [9] gave a more thorough expression for the surface tension of a pure metal as:

$$\sigma_A = k\,\Delta H_0^{sub} - RT \quad (3)$$

where ΔH_0^{sub} is the heat of sublimation of the pure material at T=0 and k is an empirical constant which are typically in the range of 0.17 to 0.20. The constant R approximates surface entropy.

The macroscopic thermodynamic model can be used for different systems such as ideal solutions, or multicomponent systems with nonregular solution behavior and varying molar areas. The major disadvantage of this model is the limitation in determining only mocroscopic surface composition and composition profiles for continous surfaces. In addition, the use of the model suffers from a lack of knowledge of how mixing properties in the surface region differ from bulk mixing behavior [9].

3.1.2. The Bond Breaking Models

These models are microscopic in nature in contrast to the macroscopic thermodynamic models. Bonds between unlike components are also treated in a chemical fashion. Bond-counting/free energy minimization approach and Monte Carlo method are two examples for the bond breaking models [9].

In bond-counting/free energy minimization approach, macroscopic composition profile can be obtained by using detailed bond energy information. If bond energies are accurately known for the surface and bulk interactions, this approach can be said to have good results for regular and near-regular solutions. In addition to that, chemisorption can be modelled. But when only bulk data are used, the results are misleading. Also, they are limited in applications as they can be applied only for flat surfaces. Size mismatches must be handled in the bond energy model. The main advantage of this model is its direct relationship with a physical picture of a surface region. From the pair-wise interaction energies, the

entropy of mixing as functions of layer composition are found and then proceded to minimize the free energy with respect to layer composition.

In the Monte Carlo method the input data needed are also detailed bond energy information and symmetrical mixing model. However, one major advantage of this method is that it can be applied to any surface and it provides detailed, microscopic composition information as well as surface ensemble behavior [9].

CHAPTER IV

METHOD

The general method of application was taken from the study of King [9]. First, the pair bond energies associated with unlike atom pairs in both the bulk and surface regions were determined from the thermodynamic mixing data and pure component properties, then the total energies of the cluster systems were predicted by using the Monte Carlo method.

Briefly, the Monte Carlo application was done as the following: Initially, the atoms were distributed randomly in the cluster, which were assumed to be in cubo-octohedral shape due to their equilibrium geometry. Two of the cubo-octahedra shaped clusters can be seen in Fig. 4.1.

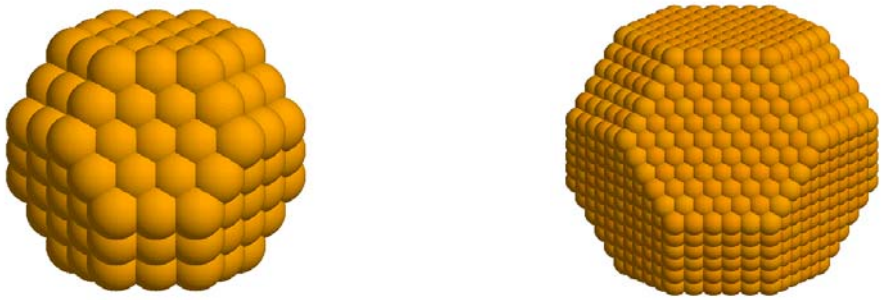

(a) Cluster with 201 atoms (b) Cluster with 2406 atoms

Figure 4.1 Clusters with cubo-octahedral structures

Then the Monte Carlo procedure was applied by picking one atom each time and calculating the least possible energy of the system due to the change in positions of the selected atom and one of its nearest neighbors. After the configurational energy is calculated and found that the new position is not energetically favorable, meaning the new system has a larger total energy than the initial system, another statistical probability is calculated according to the Boltzman distribution by exp(–$\Delta E/kT$), namely the Boltzmann factor, which is to be compared with a random number picked between zero and one. The new configuration is accepted if this quantity is larger than this random number, otherwise the initial configuration is retained. This procedure was applied to several randomly chosen atoms in the cluster several number of times until the system reaches an equilibrium that can be attributed to no significant changes in total energy.

At different temperatures ranging between 298–1000 K and at different compositions the simulations were done for Pt-IB (IB=Au, Ag, and Cu) and Pt-Pd. Each bimetallic cluter had 201, 586, 1289, and 2406 atoms, respectively. The clusters were treated in vacuo, in the absence of any kind of adsorbates.

The pairwise bond model described in King's study [9] was used because of its congruency for metal–metal bonds and metal/vacuum interfaces. The surface relaxations were not taken into account while the total configurational energy of an atom is assumed as equally distributed among its nearest-neighbor bonds. The bond distance was taken as about 3 Å (for all metals) whereas only the nearest-neighbor exchanges were considered.

Taking King's [9] study as the reference, the pair interaction energy, E_{ij}, for a bulk *i-j* pair was calculated from the related equation:

$$E_{ij} = w_{ij} / Z + (\varepsilon^{i}_{n} + \varepsilon^{j}_{m}) \qquad (6)$$

where w_{ij} / Z is the mixing energy for the *i–j* pair and independent of coordination of the participating pair atoms and temperature while *Z* is in fact the coordination number for the bulk lattice. The term $(\varepsilon^i_n + \varepsilon^j_m)$ is the energy associated with the pairwise interaction between the *i*th and *j*th atoms having coordinations *n* and *m*, respectively.

Here, each ε^i_n term can be thought as the contribution of *i*th atom to the energy of the pairwise interaction with a nearest-neighbor atom. This term has been also defined as the partial bond energy of *i*th atom and determined by an empirical expression

$$\varepsilon^i_n = a^i + b^i n + c^i n^2 \tag{7}$$

where a^i, b^i, and c^i are adjustable constants that are determined from experimental data. For the Au-Pt, Ag-Pt, and Cu-Pt clusters, the parameters derived by King [9] were used in order to check the algortihm and the computer code has been given in Appendix A. Furthermore, the algorithm has been discussed in Section 4.1. For Pt-Pd system the parameters were calculated. All of these parameters for the related systems were given in Table 4.1.

Table 4.1 Constants for the surface-modified pair potential

Metal (*i*)	a^i (eV)	b^i (eV)	c^i (eV)	Reference
Au	–0.3049	–0.025870	0.0020700	[9]
Ag	–0.2397	–0.016010	0.0013010	[9]
Cu	–0.3925	–0.001112	0.0008078	[9]
Pd	–0.1700	–0.049000	0.0030000	[29,47,48]
Pt	–0.4015	–0.052320	0.0037590	[9]

As stated by King [9], three equations, which were derived from the sublimation energy, vacancy energy and surface tension data for the related metals, were needed in order to find these constants. Therefore, sublimation and vacancy energy, suface tension and lattice constant of Pd were found from literature and used based on the theory explained below to calculate these contants. The parameters and their reference information were submitted in Table 4.2.

Table 4.2 Thermodynamic data for Pd collected from literature

Parameters		Reference
ΔH_{sub} (eV/atom)	3.9074	[47]
E_v (eV/atom)	1.26	[29]
$\sigma_{(100)}$ (eV/atom)	1.2002	[29]
a_0 (Å)	3.886	[48]

The following theory was taken as guide for calculations of the constants:
The configurational energy of a seven-atom system centered about a kink site present at the (100) plane can be shown as

$$E_0 = 12\,\varepsilon^i_{12} + 11\,\varepsilon^i_{11} + 10\,\varepsilon^i_{10} + 9\,\varepsilon^i_9 + 8\,\varepsilon^i_8 + 7\,\varepsilon^i_7 + 6\,\varepsilon^i_6 \quad (8)$$

When sublimation takes place, an atom will be removed from the kink site. According to this, six pair bonds will be broken and the configurational energies of the sublimed atom's six nearest neighbors will also be changed since the coordination number as well changes among these atoms. Therefore, the configurational energy of the system once sublimation occurs will be as

$$E_f = 11\,\varepsilon^i_{11} + 10\,\varepsilon^i_{10} + 9\,\varepsilon^i_9 + 8\,\varepsilon^i_8 + 7\,\varepsilon^i_7 + 6\,\varepsilon^i_6 \quad (9)$$

Hence, the energy change for sublimation of a single atom (ignoring *PV* effects) can be written as

$$\Delta H^{i}_{\text{sub}} / N_{\text{AV}} = E_f - E_0 = -12\ \varepsilon^{i}_{12} \tag{10}$$

where N_{AV} is the Avogadro's number. This is equivalent to the breaking of six metal–metal bonds. The same result will hold for kink site sublimation from the (110) and (111) surfaces.

Correspondingly, the energy needed to remove one atom from the bulk while leaving a vacancy, and to place this atom at a kink site can be defined as the energy of bulk vacancy formation, $E_v^{\,i}$. By counting pair bonds of the affected atoms, as above, results as

$$E_v^{\,i} = 12\ (11\ \varepsilon^{i}_{11} - 12\ \varepsilon^{i}_{12}) \tag{11}$$

Lastly, the surface energy of a (100) crystal surface can be modeled as one half the energy required to cleave a crystal along the (100) plane. It can be represented as

$$\sigma^{i}_{0(100)}\ a_0^{\,2} / 2 = 8\ \varepsilon^{i}_{8} - 12\ \varepsilon^{i}_{12} \tag{12}$$

where $\sigma^{i}_{0(100)}$ is the surface energy of *i* for a (100) surface and a_0 is the lattice constant. The calculated partial bond energies (ε^{i}_{12}, ε^{i}_{11} and ε^{i}_{8}) for Pd atom and the constants are shown in Table 4.3. For comparison, the constants used in De Sarkar et al.'s [6] study for Pt-Pd system has been also given.

Table 4.3 Derived parameters

Calculated parameters	This study		De Sarkar et al. [6]	
	Pd	Pt	Pd	Pt
w_{ijz} (eV)/Z		–0.004		–0.00396
ε_8 (eV/atom)	–0.37031	–0.57948	–0.37302	–0.58154
ε_{11} (eV/atom)	–0.326	–0.52218	–0.34785	–0.52169
ε_{12} (eV/atom)	–0.346	–0.48804	–0.3275	–0.48754
a^i	–0.17	–0.4015*	–0.17702	–0.42874
b^i	–0.049	–0.05232*	–0.04842	–0.04750
c^i	0.003	0.003759*	0.00299	0.00355

In Table 4.3, there is a derived parameter, w_{ijz}, that has not been discussed yet. In the first equation the whole term "w_{ij} / Z" was introduced as the mixing energy for the *i–j* pair. To find this parameter, a non-random mixing model similar as King's [9] model in view of the fact that the nonrandom approach is more accurate in general since no assumptions regarding clustering or ordering have to be made were used. Due to this approach, the molar excess free energy of mixing, $\Delta G_{\mathrm{mix}}^{\mathrm{ex}}$, is

$$\frac{\Delta G_{mix}^{ex}}{ZRT} = X_i X_j \frac{w_{ij}}{ZkT}\left(1 - X_i X_j \frac{w_{ij}}{ZkT}\right) \tag{13}$$

where w_{ij} actually is the so-called interchange energy which can be modified from Eqn. 6 and hence can be stated as

$$w_{\mathrm{ij}} \equiv Z\left[E_{ij} - \left(\varepsilon_n^i + \varepsilon_m^j\right)\right] \tag{14}$$

* The data are taken from reference [9]

By using Eqn. (14) and the data taken from Darby and Myles [49] this interchange energy was calculated. The literature and calculated data can be seen in Tables 4.4 and 4.5, respectively. After finding the interchange energy for each atom fraction, the final interchange energy was found by averaging all of them.

Table 4.4 Data taken from Darby and Myles [49]

XPd	G_{mix} (cal/g)	$G^{IM}_{mix}=RT\,\Sigma\, x_i \ln x_i$
0.9	–1090	–1033.50
0.8	–1740	–1590.87
0.7	–2160	–1942.05
0.6	–2420	–2139.63
0.5	–2510	–2203.65
0.4	–2450	–2139.63
0.3	–2210	–1942.05
0.2	–1790	–1590.87
0.1	–1140	–1033.50

Table 4.5 Calculated interchange energy

G_{ex} (cal/g)	w_{ij}/k (K)	w_{ij} (eV)
–56.49	$-2.27\ 10^{-3}$	–272
–149.12	$-3.37\ 10^{-3}$	–404
–217.94	$-3.75\ 10^{-3}$	–450
–280.36	$-4.22\ 10^{-3}$	–507
–306.34	$-4.43\ 10^{-3}$	–532
–310.36	$-4.68\ 10^{-3}$	–561
–267.94	$-4.61\ 10^{-3}$	–554
–199.12	$-4.50\ 10^{-3}$	–540
–106.49	$-4.28\ 10^{-3}$	–513
Average	$-4.01\ 10^{-3}$	–481

The mixing energies of Pt-IB clusters were again taken from King [9]**.** All of these were given in Table 4.6 including De Sarkar et al.'s parameter for Pt-Pd system for the chance of comparison.

Table 4.6 Mixing energies for Pt-IB and Pt-Pd pairs [6,9]

Bond pair	Mixing energy (w_{ijz}/Z) (eV/bond)	Reference
AuPt	0.0226	[9]
Ag Pt	0.0000	[9]
Cu Pt	–0.0336	[9]
Pt-Pd	–0.0040	This study
Pt-Pd	–0.00396	[6]

4.1. Algorithm

The code is constructed as a main program calling three subroutines one of which has the Monte Carlo algorithm in it, which also calls two other subroutines. The computer code in Fortran77 and the file containing the input parameters are listed in Appendices A and B, respectively. A flow-chart for the program is schematized in Fig. 4.2 and the main items of the procedure are explained in Table 4.7.

Table 4.7 Various items of the computer code and their descriptions

SUBROUTINE	Procedure	Description
MAIN	input	Input parameters are read from "mcs.5" (see Appendix B for the data)
	data check	Consistency of the input data is checked
INITIALIZE	initialize	Initializes the atomic positions, types, and all other variables are initialized according to the input file or to the predefined defaults
FINDB	find bonds	Initializes a table that contains index for each atom, index for its neighbors, and their types
MC	simulation	Total energy of the two systems, before and after the exchange of two unlike atoms, are compared. Monte Carlo decision is performed.
ENERGY	energy	Total energy of the current cluster is calculated
STATISTICS	statistics	Bond statistics, dispersion, etc. are calculated

The code requires two inputs files:

i) "mcs.5" : It contains all the input parameters and necessary data in the following form

```
 NSTEPS     ISTEP     MSKIP    MSAVER
   ISFR      IDOM      NDOM    NATOMS
      T       TOL       PER      WIJZ
    at1        a1        b1        c1
    at2        a2        b2        c2
```

A typical data is given below for a 10% Pt and 90% Pd mixed cluster of size 2406 at 800 K and with 5 million MC steps:

```
5000000    500000       100   4990000
      0         2         0      2406
  800.0       3.0      0.10    -0.004
     Pt   -0.4015 -0.052320 0.0037590
     Pd    -0.17    -0.049     0.003
```

ii) "mcs.pdb": This file contains the data for the types and coordinates of the atoms in the cluster given in ProteinDataBank (pdb) format:

```
ATOM      1  Pd  mcs c   1       0.000   0.000   0.000
ATOM      2  Pt  mcs d   2      -1.962  -1.962   0.000
ATOM      3  Pt  mcs d   2      -1.962   0.000  -1.962
ATOM      4  Pt  mcs d   2      -1.962   0.000   1.962
   ......
ATOM   2402  Pd  mcs c   1       7.848  21.583   1.962
ATOM   2403  Pt  mcs d   2       0.000  21.583  -9.811
ATOM   2404  Pt  mcs d   2      -9.811  21.583   0.000
ATOM   2405  Pd  mcs c   1       9.811  21.583   0.000
ATOM   2406  Pd  mcs c   1       0.000  21.583   9.811
```

The descriptions of the variables are given in Table 4.8.

Table 4.8 List of the variables in the input file

Variable	Description
natoms	The number of atoms in the cluster
nsteps	The number of Monte Carlo steps to be performed
istep	The number of Monte Carlo steps after which the various statistics will be printed
T	Temperature in Kelvin
isfr	This string can either be '*on*'=1 or '*off*'=0. If it is = 1: The atomic positions will be read from the pdb file, but the types will be assigned randomly according to the input variables (*idom, per, ndom*) 0: The atomic positions as well as the atomic types will be read from the pdb file, this property is necessary if an unfinished run is to be continued or to perform further relaxation.
idom	Index of dominant atomic type, only relevant in the case when *isfr* is *on*, during initalizing the atomic types randomly according to (*per* or *ndom*).
per	Percentage of the dominant atomic type, only relevant if *isfr* is *on* since during the atomic type initalization process randomly.
ndom	Number of atoms of the dominat atomic type (1 or 2), only relevant if *isfr* is *on,* while initalizing the atomic types randomly, the number of dominant atoms must be equal to *num*. To specify the dominant atom type either *ndom* or *per* can be used.
msaver	Monte Carlo step after which the output data are included in the averaging procedure
mskip	Number of random number generations to be skipped before starting the calculations. If 0, the code will set its valu randomly.

The layout of the whole program is as follows:

The type and related parameters of the atoms, their percentages, total number of atoms, temperature (in K), number of Monte Carlo steps and the other necessary data for statistics are read from the input file and the program is started:

1. The two types of atoms with thegiven percentage are randomly distrubuted in the initial cluster file.
2. The total energy of the cluster is calculated from equations (6) and (7).
3. An atom is selected randomly anywhere in the cluster, and it is replaced with one of its neighbors that is also randomly chosen, and of different type.
4. The new total energy after the exchange is calculated using the same equations.
5. The new and old total energies are compared.
6. If the new energy, E_f, is less than the old one, E_i, then the new configuration is accepted.
7. If the new energy, E_f, is greater than the old one, E_i, the Boltzmann factor $\exp(-\Delta E/kT)$ is calculated, where $\Delta E = E_f - E_i$, k is the Boltzmann constant, and T is the temperature in K.
8. A random number R is generated between 0 and 1, and is compared with the calculated Boltzmann factor.
9. If the Boltzmann factor is greater than the random number R, the new configuration is accepted. Otherwise, the old configuration is retained.
10. The same procedure is repeated from item 3 to 9 until the last Monte Carlo step is reached. The atomic arrangement that gives the minimum total energy for the cluster is kept as the final structure.

A flow-chart showing the whole procedure is given in Fig. 4.2.

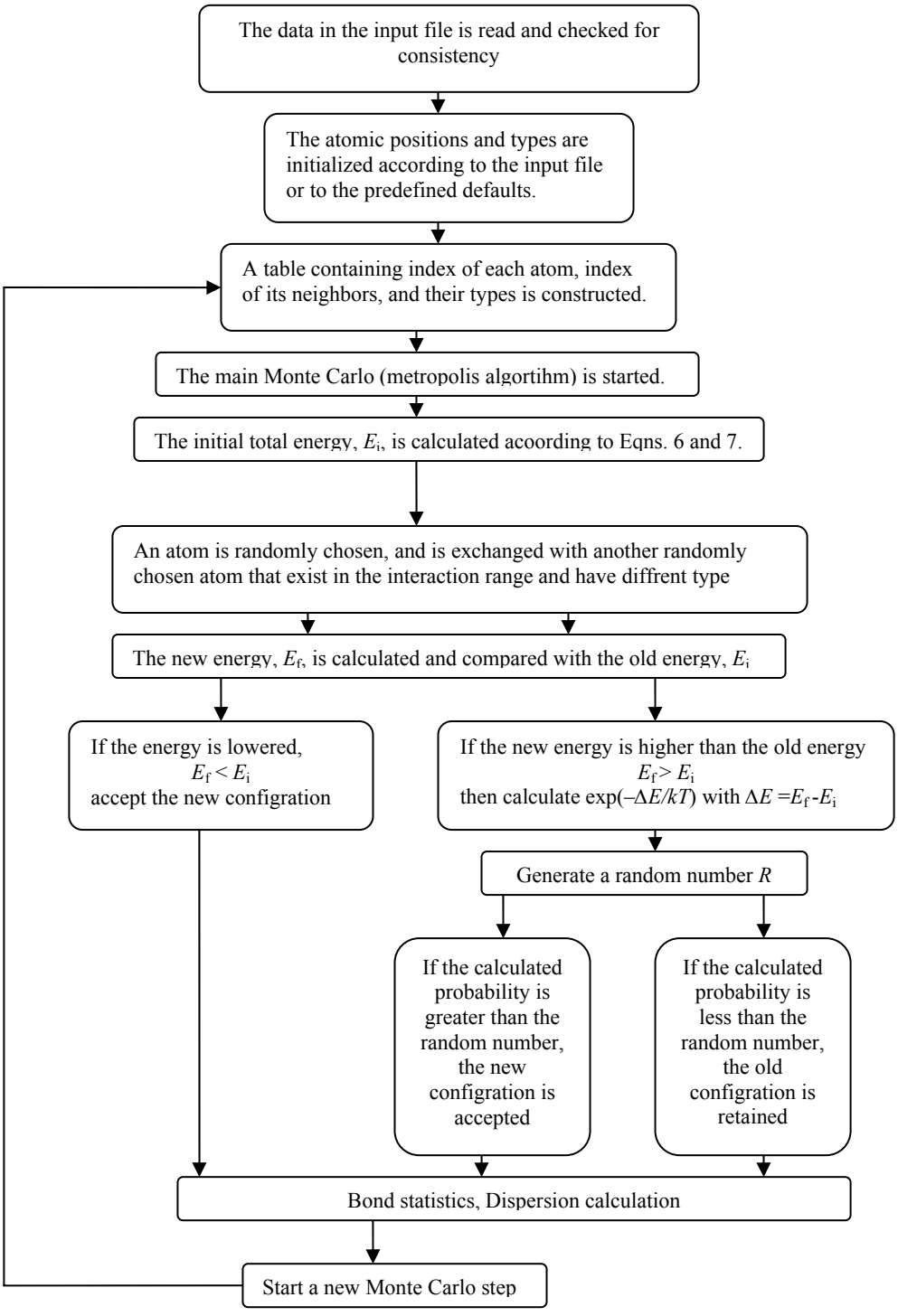

Figure 4.2 The flow-chart of the program

The cluster sizes studied in this work contained 201, 586, 1289, and 2406 atoms. In Table 4.9 the relative numbers of the atoms with respect to their coordination numbers and overall dispersions of the clusters are presented.

Table 4.9 The relative amounts of the atoms with respect to the cluster size and coordination number for cubo-octahedron structure clusters

Total number of atoms in the cluster	201	586	1289	2406
Dispersion*	0.6069	0.4642	0.3739	0.3126
6 coordinated	24	24	24	24
7 coordinated	36	72	108	144
8 coordinated	6	24	54	96
9 coordinated	56	152	296	488
12 coordinated	79	314	807	1654

* Defined as the ratio of the number of atoms on the surface to the total number of atoms

CHAPTER V

RESULTS AND DISCUSSION

A code using the coordination-dependent potential model was developed based on the work of King [9]. The algorithm of the code was explained in Chapter IV. In order to compare the predictions of the the program, Pt-IB (IB=Ag, Cu, and Au) clusters containing 201, 586, 1289 and 2406 atoms with cubo-octohedra shape were modelled at 300 K, 550 K and 1050 K as done in King's [9] study. As a second step, with the same algorithm, Pt-Pd segregation behavior was estimated. In this chapter the results and interpretations will be presented.

5.1 Verification

The results obtained from the algoritm generated in this work using the parameters presented by King [9] agreed very well with their data. The numerical results on the bulk and surface compositions of the alloys are given in Tables 5.1 and 5.2 and the structures are given in Fig. 5.1.

Table 5.1 The distribution of metal atoms between the bulk and surface for the cluster containing 2406 atoms at 550 K

IB	Composition %	$IB_{surface}/IB_{total}$	$IB_{surface}/IB_{total}$ [9]
Au	24	0.9455	0.9649
Ag	24	0.9219	0.9583
Cu	40	0.4792	0.5766

Table 5.2 Bulk and surface composition values for clusters containing 2406 atoms at 550 K

Coordination number of the site	Number of sites occupied by IB	Number of sites occupied by Pt	% occupied by IB	% occupied by Pt
System : AuPt (24% Au)				
6	24	0	1.00	0.00
7	144	0	1.00	0.00
8	92	4	0.96	0.04
9	294	194	0.60	0.40
12	15	1639	0.009	0.991
System : AgPt (24% Ag)				
6	24	0	1.0	0.00
7	143	1	0.993	0.007
8	93	3	0.97	0.030
9	271	217	0.56	0.44
12	45	1609	0.03	0.97
System : CuPt (%40 Cu)				
6	24	0	1.00	0.00
7	142	2	0.09	0.01
8	86	10	0.90	0.10
9	209	279	0.43	0.57
12	501	1153	0.30	0.70

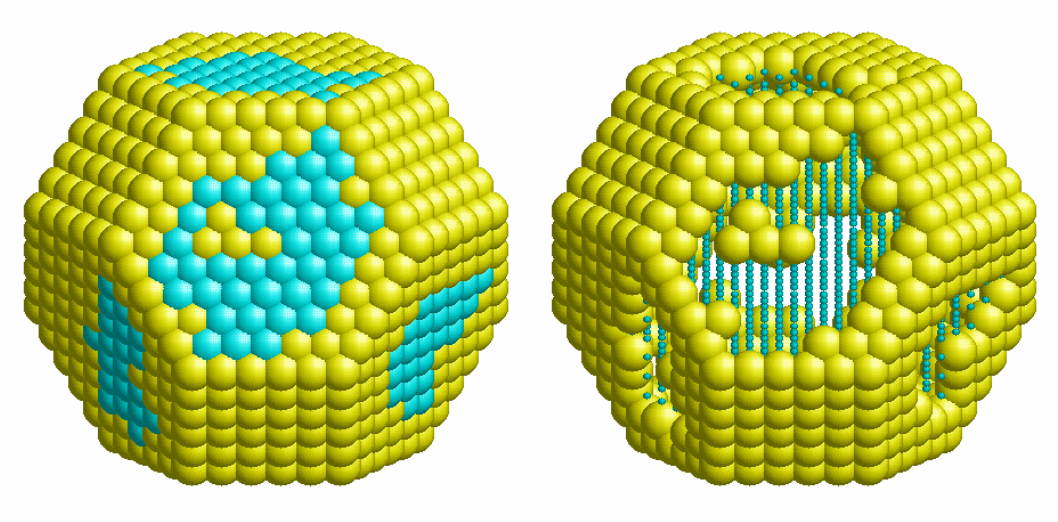

(a)

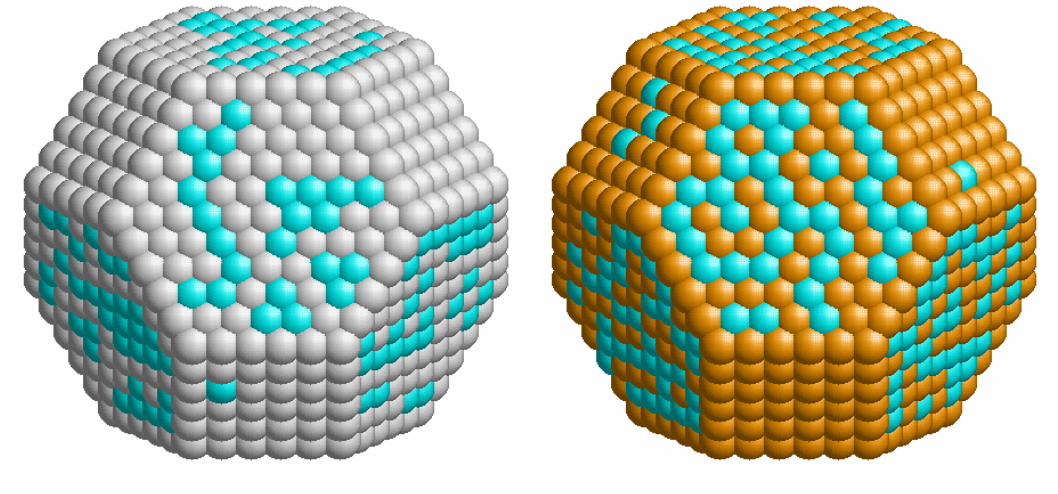

(b) (c)

Figure 5.1 Pt-IB clusters at 550 K having 2406 atoms. (a) Au-Pt System with Au atoms in yellow and Pt in blue, (b) Ag-Pt system with Ag atoms in grey and Pt in blue, and (c) Cu-Pt system with Cu atoms in red and Pt in blue

It was known that the structures of the clusters can take many forms as presented in the introduction. Based on the report on King [9], indicating that truncated cubo-octahedron is the equilibrium shape of the mono and bimetallic clustes, these structures were held fixed in this work.

Summarizing briefly, in the Au-Pt system, Au and Pt atoms segregated due to their endothermic mixing energy. For the Cu-Pt system, Cu and Pt atoms were found to be mixed and formed a miscible alloy which was also an expected result due to their exothermic mixing energy. Lastly, the random distibution of Ag and Pt atoms in Ag-Pt system was in good agreement with their nearly zero mixing energy quantity, as well.

In his work, King [9] also said that the degree of clustering of Pt atoms on the surface of the catalyst particles depends on which IB element is present as for Au-Pt system having to produce larger ensembles of surface Pt atoms than the Ag-Pt or Cu-Pt systems. This consequence was supported in our study, too. He also recorded that generally IB segregated to the surface of the catalyst in Pt-IB systems and tend to the lowest coordinated site first and this situation was verified in our study as well.

As King [9] recorded that amongst IB atoms, Au was the most segregated to surface, in our study this was observed, too. It can be seen more clearly in Fig 5.2. In this figure, the effect of cluster size can be seen clearly, as well. The increasing of cluster size results in decreasing of Pt atoms on the surface for each system.

As a result, our findings have supported the previous work of King's for Pt-IB clusters [9]. Therefore, the code is used for the second part of this study, namely in modelling of Pt-Pd clusters.

5.2 Predictions on Pt-Pd Bimetallics

The effects of bimetallic catalysts enhance the catalytic activity for certain reactions were mentioned in previous sections. Nowadays, palladium is known best for potential applications both as a catalyst in heterogeneous catalysis, because of its sulphur and nitrogen poisoning resistance, and in membranes for hydrogen separation [6, 25]. However, Pd tends to have low dispersions and this can be a disadvantage. Therefore, to increase its dispersion, a synergistic effect can be created from a metal that has high dispersion value. From the H_2 chemisorption experiments done by Kaya [18]**,** it was shown that supported Pd had low dispersions while Pt had high dispersion values. (His results are given in Table 5.5.) He also showed that for the co-impregnated Pt-Pd catalysts the dispersions were higher. The aim of this study is to determine whether one can make a better catalyst utilizing the catalytical properties of Pd and the high dispersion property of Pt at the same time. Hence, Pt-Pd bimetallic catalysts were modeled for different dispersions and compositions at different temperatures in order to observe the potential active sites on a cubo-octahedral shaped structure. The modelled clusters are shown in Fig. 5.2 and the numerical results on the bulk and surface compositions of the clusters are given in Tables 5.3 and 5.4.

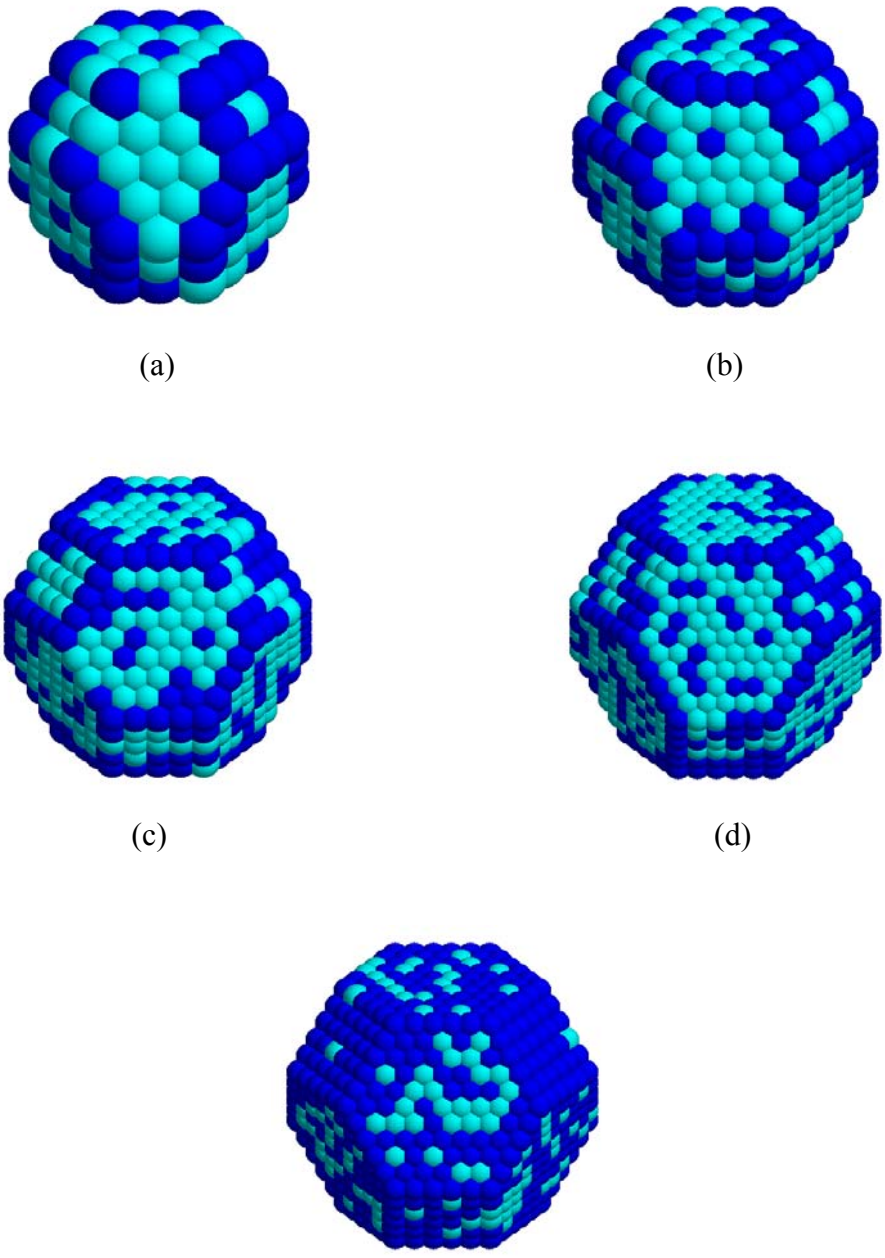

Figure 5.2 Pt-Pd clusters at 800 K with 25% Pd content. (a) 201-atom cluster, (b) 586-atom cluster, (c) 1289-atom cluster, and (d) 2406-atom cluster. Finally, (e) 2406-atom cluster with 50% Pd content. Pd atoms are shown in cyan and Pt atoms are in blue

Table 5.3 Bulk and surface composition values for Pt-Pd cluster containing 2406 atoms at 800 K

Coordination number of the site	Number of sites occupied by Pd	Number of sites occupied by Pt	Pd fraction of the site
10% Pd			
6	20	4	0.833
7	74	70	0.514
8	25	71	0.260
9	48	440	0.098
12	74	1580	0.045
25% Pd			
6	22	2	0.917
7	113	31	0.785
8	55	41	0.573
9	147	341	0.301
12	265	1389	0.160
50% Pd			
6	23	1	0.958
7	133	11	0.924
8	83	13	0.865
9	298	190	0.611
12	666	988	0.403
75% Pd			
6	24	0	1.000
7	144	0	1.000
8	93	3	0.969
9	417	71	0.855
12	1126	528	0.681

Table 5.4 Bulk and surface composition values for Pt-Pd clusters with 25% Pd content at 800 K

Coordination number of the site	Number of sites occupied by Pd	Number of sites occupied by Pt	Pd fraction of the site
Total number of atoms :2406			
6	22	2	0.917
7	113	31	0.785
8	55	41	0.573
9	147	341	0.301
12	265	1389	0.160
Total number of atoms :1289			
6	23	1	0.958
7	88	20	0.815
8	19	35	0.352
9	87	209	0.294
12	106	701	0.131
Total number of atoms :586			
6	24	0	1.000
7	57	15	0.792
8	8	16	0.333
9	25	127	0.165
12	33	281	0.105
Total number of atoms :201			
6	22	2	0.917
7	23	13	0.639
8	1	5	0.167
9	5	51	0.098
12	0	79	0.000

In Figures 5.3 and 5.4, a comparison with experimental results of the predictions for Pd-rich (80% Pd) and Pt-rich (80% Pt) systems at various temperatures can be seen. The results are given for both the 201- and 2406-atom cluster. When Pd-rich case is investigated, it was found thar for 2406-atom containing and experimental results, after 700 K a slight decrease took place, then as the temperature rises both predictions and experimental results seem to have closer compositions on the surface.

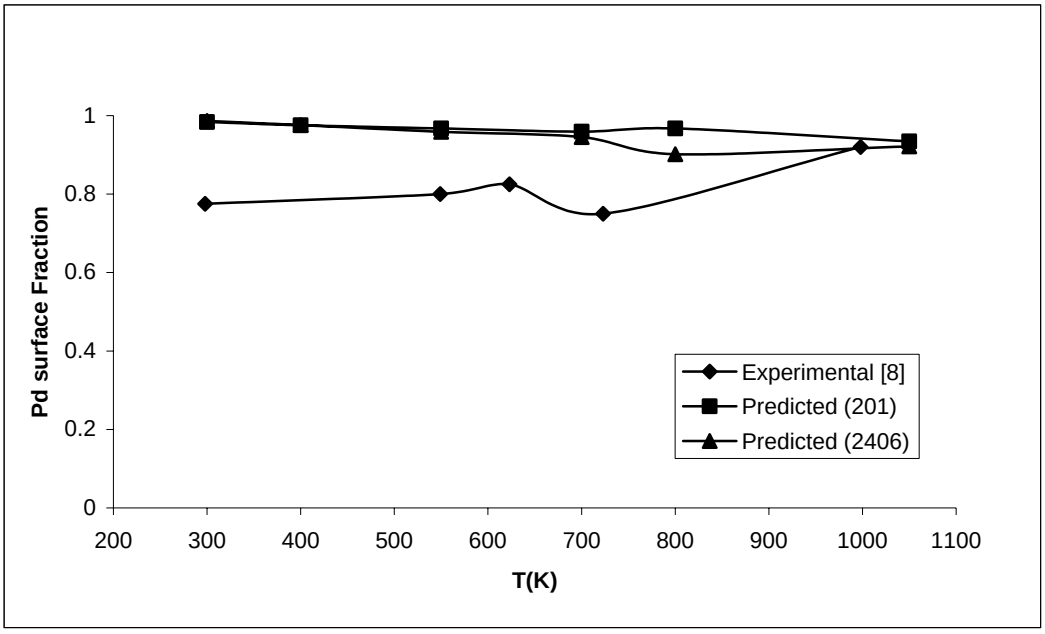

Figure 5.3 Predicted (201 and 2406-atom cluster) and experimental results for 80% Pd-containing Pt-Pd system at different temperatures

However for Pt-rich case the predictions and the experimental results showed difference. Actually, an oscillation-like behavior observed in the experimental results. For predictions, the highly dispersed cluster (201 atom containing) showed nearly a constant bevior while a decrease in surface coverage wiht Pd atoms up to 700 K and an increase was observed for the other cluster.

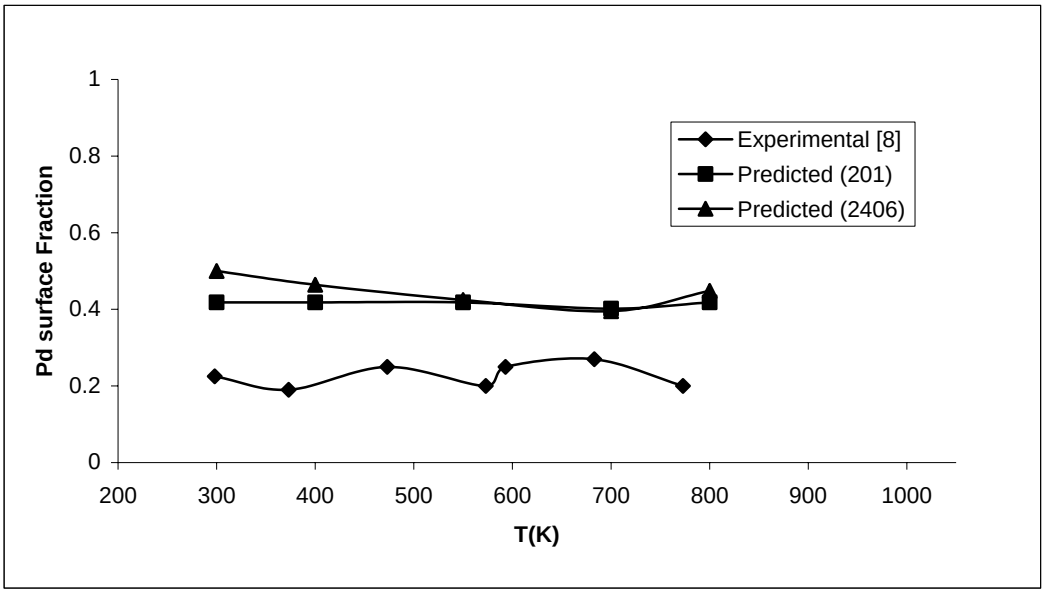

Figure 5.4 Predicted (201 and 2406-atom cluster) and experimental results for 20% Pd-containing Pt-Pd system at various temperatures

The dispersion versus surface average of Pd at 800 K graph was given in Fig. 5.5. As it can be seen, the surface average composition is almost independent of dispersion.

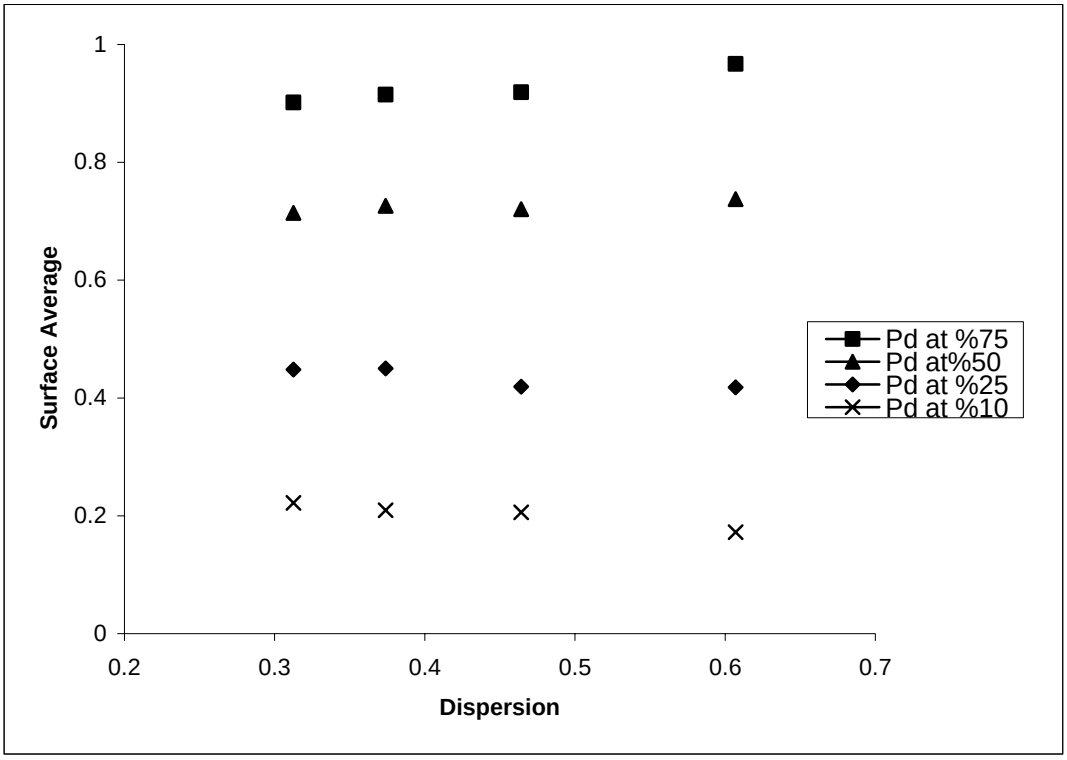

Figure 5.5 Dispersion versus surface average fraction of Pd at 800 K

When the surfaces of the clusters were observed and compared with Rousset et al.'s study [29], it was found that the predictions under estimated for the compositions of (111) and (100) sites especially for low Pd concentrations. The predictions were performed for 201 atom containing clusters at 800 K for different compositions. The compared results are given in Figs 5.6 and 5.7.

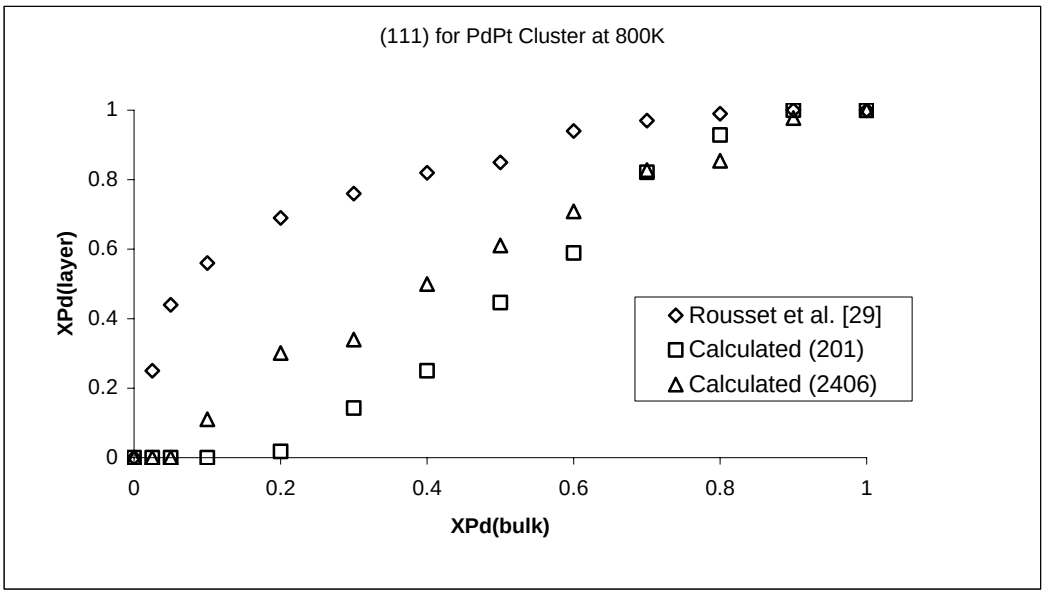

Figure 5.6 Comparison of 201 and 2406-atom cluster with Rousset et al.'s results for (111) sites at 800 K

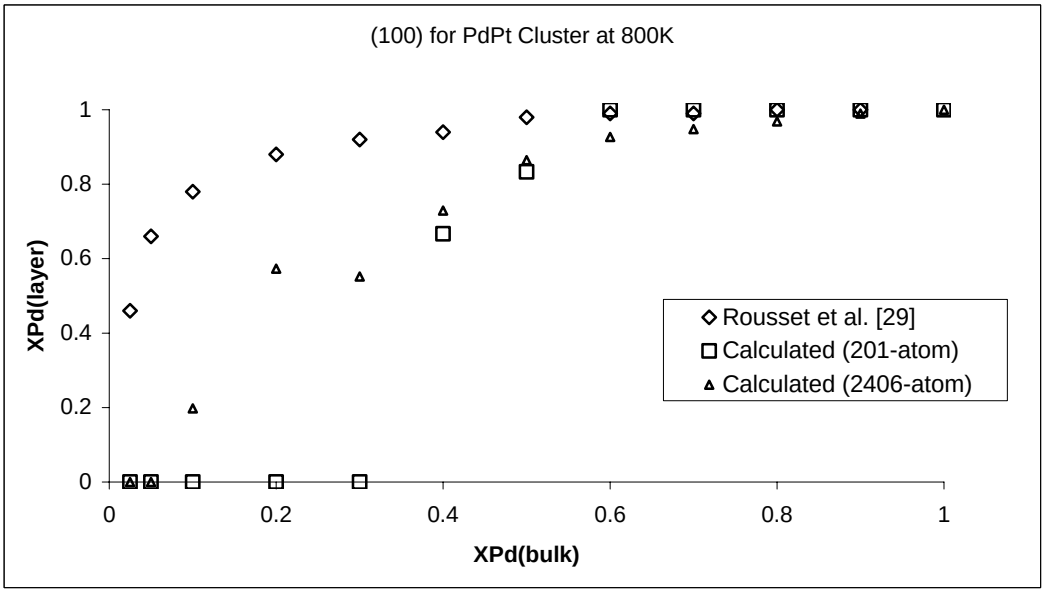

Figure 5.7 Comparison of 201 and 2406-atom cluster with Rousset et al.'s results for (100) sites at 800 K

These under estimations emanated from the differences of the methods used and the differences in the structure. In their study, they considered surface relaxations due to low coordinated sites on infinite surfaces. In clusters containing finite number of atoms, the population of the planes could not be observed at low Pd concentrations due to the fact that the defect like sites are populated first.

Pd atom containing sites have been given in more detailed in Fig. 5.8. For a 2406 atom containing cluster at 800 K, Pd occupying sites are shown.

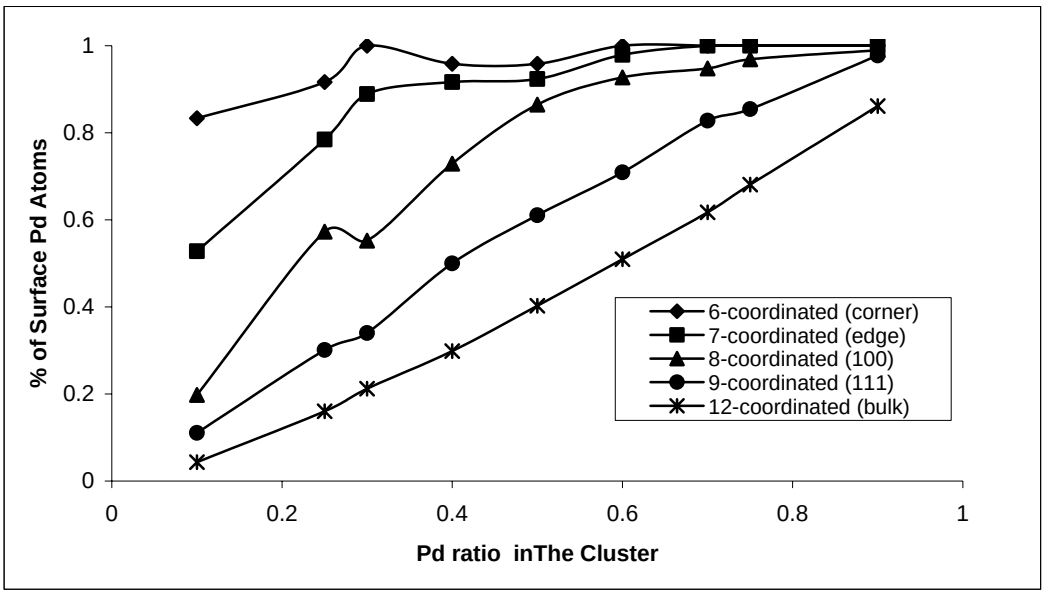

Figure 5.8 Pd atoms occupying various sites of 2406-atom cluster at 800 K

As it is seen at low bulk Pd fractions, surface atoms were populated at the edge and corner sites. As more Pd became available, population at low index planes increases.

In Table 5.5 the dispersion data of Kaya [18] is presented. In his work, Kaya prepared 1 wt% metal containing bimetallic catalysts, he measured the dispersions by volumetric chemisorption technique and measured the activity of the catalysts towards CO oxidation reaction. On the same table, the approximate cluster size and average surface Pd amounts determined based on the results obtained in this work are also presented.

Table 5.5 The dispersions of 1 wt% metal/Al_2O_3 Pt-Pd bimetallic catalysts determined by volumetric hydrogen chemisorption technique [18]

Catalyst	at.% Pd	% overall dispersion by volumetric chemisorption technique [18]	Average cluster size chosen based on the dispersion	Overall dispersion of the cluster	Pd dispersion (*)	% of the surface sites occupied by Pd
1 wt% Pt/Al_2O_3	0	70.4	201	0.6069	0.00	0.00
1 wt% $Pd\text{-}Pt/Al_2O_3$	25	57.8	201	0.6069	1.00	0.42
1 wt% $Pd\text{-}Pt/Al_2O_3$	50	52.3	586	0.4642	0.67	0.72
1 wt% $Pd\text{-}Pt/Al_2O_3$	75	49.1	586	0.4642	0.57	0.91
1 wt% Pd/Al_2O_3	100	47.9	1289	0.3739	1.00	1.00

(*) Pd dispersions were determined as the ratio of Pd atoms on the surface to the total Pd atoms present in the bimetallic cluster.

As can be seen from the data presented in Table 5.5, the monometallic Pd dispersions are very high in bimetallic systems especially at low Pd loadings. All of the Pd atoms are on the surface for the catalysts with 25% Pd loading. As the Pd loading increased the average cluster size increased which decreased the relative coverage of the defect-like sites, hence the surface coverage of Pd decreased. This effect has been nicely observed by Kaya [18] in terms of CO

oxidation kinetics. His bi-metallic light-off data for all Pd containing catalysts coincided with the monometallic Pd indicating that surface sites effective in CO oxidation reaction (defect-like sites) were occupied by Pd atoms.

CHAPTER VI

CONCLUSION

A program was generated to model the atom distributions in bimetallic clusters based on the work of King [9]. The predictions of the program were verified against the previously predicted Pt-IB system as well as Pt-Pd system where both experimental and theoretical predictions are available.

The program predicted that Pd atoms were segregated on the surface of the Pt-Pd catalysts. Since Pd metals are good for sulphur and nitrogen poisining in various reactions, including hyrogenation reactions, their performance can be increased by using them with Pt atoms which are known to have high dispersions.

With these examples, the accuracy of the code was established. The code can be used further with other fcc bi- or tri-metallic systems of popular interest. Furthermore, the predictions of the Monte Carlo Simulations can be used as input data for predictions in CPU demanding calculations such as DFT.

REFERENCES

[1] Jongpatiwut, S., Li, Z., Resasco, D. E., Alvarez, W. E., Sughrue, E. L., Dodwell, G. W., Applied Catalysis A: General **262**, 241–253 (2004)

[2] Cubaoctahedron (image), http://upload.wikimedia.org/wikipedia/commons/5/5e/Cuboctahedron.jpg (last accessed 14.May.2006)

[3] Truncated-octahedron (image), http://upload.wikimedia.org/wikipedia/commons/2/20/Truncatedoctahedron.jpg (last accessed 14.May.2006)

[4] Icosahedral and decahderal (image), http://www.phys.canterbury.ac.nz/research/nano/images/3structures.jpg (last accessed 14.May.2006)

[5] Persson, K., Ersson, A., Jansson, K., Iverlund, N., Jaras, S., Journal of Catalysis **231**, 139–150 (2005)

[6] De Sarkar, A., Menon, M., Khanra, B.C., Applied Surface Science **182**, 394–397 (2001)

[7] Smale,J.H., Catalysis Letters **9**, 159–172 (1991)

[8] Van den Oetelaar, L. C. A., Nooij, O. W., Oerlemans, S., Van der Gon, A. W. D., Brongersma, H. H., Lefferts, L., Roosenbrand, A. G., Van Veen, J. A. R., J. Phys. Chem. B **102**, 3445–3455 (1998)

[9] King, T. S., *Bond-Breaking and Chemical Thermodynamic Models of Surface Segregation*, Iowa State University, Iowa (1988)

[10] Deng, Y., An, L., Appl. Catal. A **119**, 13-22 (1994)

[11] Deganello, G., Duca, D., Liotta, L. F., Martorana, A., Venezia, A.M., Benedetti, A., Fagherazzi, G., J. Catal.**151,** 125–134 (1995)

[12] Vigneron, S., Deprelle, P., Hermia, J. Catal. Today **27,** 229–236(1996)

[13] Koscielski, T., Karpinski, Z., Paal, Z. J. Catal. **77,** 539–549 (1982)

[14] Attard, G.A., Price R., Surf. Sci. **335,** 63–74 (1995)

[15] Cho, S. J., Kang, S. K., Catalysis Today **93–95**, 561–566 (2004)

[16] Coq, B., Figueras, F., Journal of Molecular Catalysis A: Chemical **173**, 117–134 (2001)

[17] Chung, Y. M., Rhee, H. K., Catalysis Letters **85**, 159–164 (2003)

[18] Kaya, S., *CO Oxidation on Alumina Supported Pd-Pt Mono- and Bimetallic Catalysts: Temperature Hysteresis*, Middle East Technical University, Ankara (2002)

[19] Du Plessis, J., Taglauer, E., Surf. Interf. Anal. **22,** 556 (1994)

[20] Du Plessis, J., Van Wyk, G.N., Taglauer, E., Surf. Sci. **220**, 381–390 (1989)

[21] Hansen, P. L., Molenbroek, A. M., Ruban, A. V., J. Phys. Chem. B **101**, 1861 (1997)

[22] Rades, T., Polisset-Thofin, M., Fraissard, J., Topics in Catalysis **11/12,** 283–287 (2000)

[23] Rousset, J. L., Cadrot, A. M., Lianos, L., Renouprez, A. J., Eur. Phys. J. D **9**, 425 (1999)

[24] Overview of Computational Chemistry, http://www.shodor.org/chemviz/overview/ccbasics.html (last accessed 14.May.2006)

[25] Løvvik, O. M., Surface Science **583,** 100–106 (2005)

[26] Neyman, K. M., Illas, F., Catalysis Today **105**, 2–16 (2005)

[27] Cox, H., Surface Science, **397**, 374–381 (1998)

[28] Murrell, J. N., Mottram, R. E., Mol. Phys. **69,** 571 (1990)

[29] Rousset, J. L., Bertolini, J. C., Miegge, P., Physical Review B **53**, 4947–4957 (1995)

[30] Massen, C., Mortimer-Jones, T. V., Johnston, R. L., J. Chem. Soc., Dalton Trans., 4375–4388 (2002)

[31] Gijzeman, O. L. J., J. Catal. **92**, 409 (1985)

[32] Rousset, J. L., Stievano, L., Cadete Santos Aires, F. J., Geantet, C., Renouprez, A. J., Pellarin, M., J. Catal. **202,** 163 (2001)

[33] Molecular Dynamics and Monte Carlo, http://www.ccl.net/cca/documents/molecular-modeling/node9.html (last accessed 14.May.2006)

[34] Donnelly, R. G., King T. S., Surf. Sci. **74,** 89 (1978)

[35] Strohl, J. K., King, T. S., Journal of Catalysis **116,** 540–555 (1989)

[36] Drchal, V., Pasturel, A., Monnier, R., Kudrnovsky, J., Weinberger, P., Computational Materials Science **15,** 144–168 (1999)

[37] Khanra, B. C., Menon, M., Physica B **291,** 368–372 (2000)

[38] Deng, H., Hu, W., Shu, X., Zhao, L., Zhang, B., Surface Science **517**, 177–185 (2002)

[39] Fuggle, J. C., Hillebrecht, F. U., Zeller, R., Zolnierek, Z., Bennett, P. A., Freiburg, Ch., Phys. Rev. B **27,** 2145 (1982)

[40] Strohl, J. K., King, T. S., J. Catal. **118**, 53 (1989)

[41] Wang, G., Van Hove, M. A., Ross, P. N., Baskes, M. U., J. Phys. Chem. B **109**, 11683–11692 (2005)

[42] Zhu, L., DePristo, A. E., Journal of Catalysis **167,** 400– 407 (1997)

[43] Yang, L., DePristo, A. E., J. Catal. **148**, 575 (1994)

[44] Ramaswamy, V., Nix, W. D., Clemens, B. M., Scripta Materialia **50**, 711–715 (2004)

[45] Kuijers, F. J., Tieman, B. M., Ponec, V., Surf. Sci. **75**, 657 (1978)

[46] Overbury, S. H., Bertrand, P. A., Somorjai, G. A., Chemical Reviews **75,** 547–560 (1975)

[47] Campbell, C. T., Starr, D. E., J. Am. Chem. Soc. **124**, 31 (2002)

[48] KASZKUR, Z.(1998). *Powder diffraction of small Pd crystallites* [online] ichf.edu.pl/res/res_en/lab_xrd/LabXRD_files/parmapub.htm (last accessed 14.May.2006)

[49] Darby, J. B., Myles, K. M., Metallurgical Transactions **3**, 653 (1972)

APPENDIX A

THE COMPUTER CODE

App.A.1. The Main Code

```
C----------------------
C     PROGRAM CATALYSIS
C----------------------
C     Parameters
C     NSTEPS=5000000   number of monte carlo steps
C     ISTEP=1 < NSTEPS will print the total energy in the output
c                      file for every other istep mc steps
C     MSKIP=0          arbitrary integer number >= 0
c                      # of random number iterations to be skipped
c                       before the calculations start, if it is set
c                       to zero, code will set its value randomly)
C     MSAVER=900 < NSTEPS Monte Carlo step after which the
C                       calculation of averages will start
C     ISFR=1           if 1, atomic types are set randomly
C                       if 0, start from the initial file "mc0.pdb"
C     NATOMS=2406—201  number of atoms in the cluster
C     NDOM=0 <= NATOMS the number of dominant atoms
c                       in the alloy (neglected if ISFR=1)
C     IDOM=2           type of dominant element in the alloy
c                      (important if PER or NDOM /= 0 and ISFR=1)
C     PER=0.60  [0,1]  the percentage of dominant atoms
c                       in the alloy (neglected if ISFR=1)
C     NN=12            maximum expected number of nearest nighbors
C     TOL=3.0          maximum distance between any two atoms
c                       to be considered as nearest nighbors
c                      (Bond length for Pt, b=3.9242A/sqrt2,
c                       is used for all, as a scale. TOL > b)
C     T=1.0            Absolute temperature in Kelvin
C     AT(1)='Au'
C     AT(2)='Pt'
C----------------------

      parameter(na=2406,nnt=12)
      IMPLICIT REAL*8(A-H,O-Z)
      character*2 at(2)
      integer*4 today1(3),now1(3),today(3),now(3)
      dimension atom(3,na),v(nnt,5),coord(na,nnt)
      dimension a(2),b(2),c(2),ntype(na),neighh(na)
      open(unit=5, file='mcs.5', status='old')
```

```
      open(unit=6, file='mcs.6', status='old')
      open(unit=7, file='mcs.pdb', status='old')
      open(unit=9, file='mc0.pdb', status='old')
      NN=nnt

      read(5,10) nsteps,istep,mskip,msaver
      read(5,10) isfr,idom,ndom,natoms
   10 format(4I10)
      read(5,20) T,tol,per,wijz
   20 format(4f10.4)
      read(5,30) at(1),a(1),b(1),c(1)
      read(5,30) at(2),a(2),b(2),c(2)
   30 format(8x,a2,3f10.7)

      if(isfr.eq.1) go to 35
      do 33 i=1,1000000
   33 read(6,*,end=35)
   35 continue

      call datetime(today,now)
      write(6,*) 'Monte Carlo Output'
      write(6,40) today(2),today(1),today(3),now
   40 format(' Start ',i2,'/',i2,'/',i4,'; Time ',
     &       i2,':',i2,':',i2)
      if(now(3).eq.0) now(3)=1
      if(now(2).eq.0) now(2)=1
      mskip1=mskip
      if(mskip1.eq.0) mskip1=now(3)*now(2)
      do 50 i=1,mskip1
      randm=rand()
   50 continue
c---- decorations of output file
      write(6,*) '-----------------------------------'
      write(6,*) 'Summary of input data'
      write(6,*) 'Temperature   =',T
      write(6,*) '# of MC steps =',nsteps
      write(6,*) '# of atoms    =',natoms
      write(6,*)
     &     'Energy will be printed after every',istep,' step(s)'
      write(6,*) 'Tolerance of nearest neighbors = ',TOL
      write(6,*) 'Max # of nearest neighbors to be considered',NN
      write(6,*)
      write(6,*) 'Potential Parameters for ',at(1),' and ',at(2)
      write(6,*)
     &     'with ',at(1),' as type 1 and ',at(2),' as type 2'
      write(6,*)
      write(6,*) 'a  =',a
      write(6,*) 'b  =',b
      write(6,*) 'c  =',c
      write(6,*) 'wij/z=',wijz
      write(6,*) '-----------------------------------'
      write(6,*) '# of random number iterations skipped before'
      if(mskip.eq.0) then
      write(6,*) 'begining to the calculations chosen randomly',
     &           now(3)*now(2)
```

```
      else
      write(6,*) 'begining the calculations is chosen to be',mskip
      endif

      write(6,*) '---------------------------------'
      if(T.lt.0.or.natoms.le.0.or.msaver.gt.nsteps.or.istep.gt.
     &   nsteps.or.per.lt.0.or.per.gt.1.or.idom.lt.1.or.idom.gt.
     &   2.or.isfr.lt.0.or.isfr.gt.1.or.ndom.gt.natoms) then
      write(6,*) 'Some input parameters are not consistent'
      CALL datetime(today,now)
      write(6,60) today(2),today(1),today(3),now
   60 format('Stop ',i2,'/',i2,'/',i4,'; Time ',i2,':',i2,':',i2)
      stop
      endif

      if(per.gt.0.and.ndom.gt.0) then
      write(6,*) 'PER and NDOM are not consistent'
      CALL datetime(today,now)
      write(6,60) today(2),today(1),today(3),now
      stop
      endif

c-----------------------------------------------
c     initialize input data and generate mc0.pdb
c-----------------------------------------------
      if(isfr.eq.0) then
      n1=0
      n2=0
      matoms=0
      do 70 i=1,2410
      read(7,80,end=85) ntype(i),atom(1,i),atom(2,i),atom(3,i)
      if(ntype(i).eq.1) n1=n1+1
      if(ntype(i).eq.2) n2=n2+1
      matoms=matoms+1
   70 continue
   80 format(24x,i2,4x,3f8.3)
   85 if(matoms.ne.natoms) then
      write(6,*) 'wrong size cluster mc0.pdb'
      go to 130
      end if
      sn1=n1/float(natoms)*100
      sn2=n2/float(natoms)*100
      write(6,90) n1,sn1,n2,sn2
   90 format(' Calculations start from the resumed file'/
     &       '  with NDOM, IDOM, PER values are ignored'/
     &       '  type 1 atoms =  ',I4,' which is',f6.2,' %'/
     &       '  type 2 atoms =  ',I4,' which is',f6.2,' %')
      if(n1.eq.0.or.n2.eq.0) then
      write(6,*) 'Pure element, not an alloy!'
      goto 130
      endif
      else
      CALL initial(natoms,atom,ntype,per,idom,at,ndom)
      endif
      write(6,*) '-----------------------------'
```

```
      write(6,*)

c     calculate nearest neighbor lists
c-----------------------------------------------
      do 100 i=1,natoms
      CALL FINDB(I,NATOMS,ATOM,v,NEIGH,TOL,NN)
      neighh(i)=NEIGH
      do 100 j=1,NN
      coord(i,j)=v(j,4)
  100 continue

c     monte carlo simulation
c-----------------------------------------------
      call mc(nsteps,neighh,nn,coord,ntype,natoms,
     &               a,b,c,wijz,T,istep,msaver)
c-----------------------------------------------
c     generate the output file "mcs.pdb"
      rewind 7
      do 110 i=1,natoms
      ni=ntype(i)
  110 write(7,120) i,at(ni),ni,atom(1,i),atom(2,i),atom(3,i)
  120 format('ATOM',I7,2x,a2,'  mcs d  ',i2,4x,3f8.3)
      close(5)
      close(6)
      close(7)
      close(9)
  130 stop
      end

c-------------------------------------------------------
      SUBROUTINE initial(na,atom,ntype,per,idom,at,ndom)
c-------------------------------------------------------
      IMPLICIT REAL*8(A-H,O-Z)
      dimension atom(3,na),ntype(na)
      character*2 at(2)
      natoms=na
      n1=0
      n2=0
      do 10 i=1,natoms
   10 ntype(i)=0
      do 20 i=1,natoms
   20 read(9,30) atom(1,i),atom(2,i),atom(3,i)
   30 format(30x,3f8.3)
      ndom1=ndom
      if(per.eq.0.and.ndom.eq.0) goto 100
      if(ndom.eq.0) ndom1=int(per*natoms)+1
      do 60 i=1,ndom1
   50 irand=natoms*rand()
      if(ntype(irand).ne.0) goto 50
      ntype(irand)=idom
   60 continue
      if(idom.eq.1) io=2
      if(idom.eq.2) io=1
      do 90 i=1,natoms
      if(ntype(i).eq.0) ntype(i)=io
```

```
   90 continue
      goto 120
c     verify per
  100 do 110 i=1,natoms
  110 ntype(i)=1+anint(rand())
  120 do 130 i=1,natoms
      if(ntype(i).eq.1) n1=n1+1
      if(ntype(i).eq.2) n2=n2+1
  130 continue
      sn1=n1/float(natoms)*100
      sn2=n2/float(natoms)*100

      if(per.eq.0.and.ndom.eq.0) then
      write(6,*) 'Alloy generated completely randomly as'
      else
      write(6,*)
     &   'Alloy generated randomly with the constraint that'
      endif
      write(6,140) n1,sn1,n2,sn2
  140 format(' type 1 atoms =  ',I4,' which is',f6.2,' %'/
     &       ' type 2 atoms =  ',I4,' which is',f6.2,' %')

      rewind 9
      do 150 i=1,natoms
      ni=ntype(i)
  150 write(9,160) i,at(ni),ni,atom(1,i),atom(2,i),atom(3,i)
  160 format('ATOM',I7,2x,a2,'  mcs c  ',i2,4x,3f8.3)
      end

c-----------------------------------------------------
      SUBROUTINE FINDB(Irand,NA,ATOM,V,NEIGH,TOL,NN)
C-----------------------------------------------------
      IMPLICIT REAL*8(A-H,O-Z)
      DIMENSION ATOM(3,na),V(NN,5)
      natoms=na
      N=NN
      R2=TOL*TOL
      NEIGH=0
      DO 10 I=1,N
      DO 10 J=1,5
   10 V(I,J)=0.0
      DO 100 IS=1,NATOMS
      IF(IS.EQ.Irand) GO TO 100
      D=0.0
      DO 40 J=1,3
      RL=ATOM(J,IS)-ATOM(J,Irand)
   30 IF(ABS(RL).GT.TOL) GO TO 100
   40 D=D+RL*RL
      IF(D.GT.R2) GO TO 100
      IP=1
      IF(NEIGH.EQ.0) GO TO 80
      DO 50 IP=1,NEIGH
      IF(V(IP,5).GT.D) GO TO 60
   50 CONTINUE
      IF(NEIGH.EQ.N) GO TO 100
```

```
      IP=NEIGH+1
      GO TO 80
   60 IF(IP.EQ.N) GO TO 80
      DO 70 I=IP,N-1
      II=N+IP-I
      DO 70 J=1,5
   70 V(II,J)=V(II-1,J)
   80 DO 90 J=1,3
   90 V(IP,J)=ATOM(J,IS)
      V(IP,4)=IS
      V(IP,5)=D
      IF(NEIGH.LT.N) NEIGH=NEIGH+1
  100 CONTINUE
      RETURN
      END

c-------------------------------------------------------
      SUBROUTINE mc(nsteps,neighh,nnn,coord,ntype,nna,
     &                     a,b,c,wijz,T,istep,msaver)
c-------------------------------------------------------
      parameter(na=2406,nnt=12)
      IMPLICIT REAL*8(A-H,O-Z)
      integer*4 today1(3),now1(3),today2(3),now2(3)
      dimension a(2),b(2),c(2),atom(3,na),coord(na,nnt)
      dimension ntype(na),ntype1(na),neighh(na)
      dimension nnsum(nnt),nnsp(nnt),nnsa(nnt)
      dimension mmsum(nnt),mmp(nnt),mma(nnt)
      data bk/8.63125D-5/
      bkt=bk*T
      natoms=nna
      n=nnn

      write(6,*) '            ========= Results ========='
      write(6,*)
     &     '     Step   Total Energy    Energy Diff       Time'
      write(6,*)
     &     '     ----   ------------    -----------     --------'

      call statistics(neighh,ntype,natoms,n,nnsp,mmp)
      call energy(ntype,natoms,neighh,coord,n,a,b,c,wijz,etot1)

      do ii=1,n
      nnsum(ii)=0
      mmsum(ii)=0
      enddo

      imin=0
      esum=0
      epre=etot1
      emin=etot1

      do 90 i=1,nsteps
   20 irand1=natoms*rand()
      if(irand1.eq.0) goto 20
   30 j1=neighh(irand1)*rand()
```

```
      if(j1.eq.0) goto 30

      j=coord(irand1,j1)
      it1=ntype(irand1)
      it2=ntype(j)
      if(it1.eq.it2) goto 20
      ntype(irand1)=it2
      ntype(j)=it1

      call energy(ntype,natoms,neighh,coord,n,a,b,c,wijz,etot)

      if(etot.le.etot1) then
      etot1=etot
      goto 50
      endif

      deltae=etot1-etot
      boltz=exp(deltae/bkt)
      xxx=rand()
      if(boltz.gt.xxx) then
      etot1=etot
      goto 50
      endif

      ntype(irand1)=it1
      ntype(j)=it2

   50 if(mod(i,istep).eq.0) then
      call datetime(today2,now2)
      diff=etot1-epre
      if(dabs(diff).gt.1.e-7) write(6,60) i,etot1,diff,now2
   60 format(i10,2f15.7,5x,i2,':',i2,':',i2)
      epre=etot1
      endif

      if(etot.lt.emin) then
      emin=etot1
      imin=i
      do 70 ii=1,natoms
      ntype1(ii)=ntype(ii)
   70 continue
      endif

c     averages
      if(i.gt.msaver) then
      esum=esum+etot1

      call statistics(neighh,ntype,natoms,n,nnsa,mma)

      do 80 ii=1,n
      nnsum(ii)=nnsum(ii)+nnsa(ii)
      mmsum(ii)=mmsum(ii)+mma(ii)
   80 continue
      endif
   90 continue
```

```
    kkk=nsteps-msaver
    eaver=esum/float(kkk)
    do 100 ii=1,n
    nnsum(ii)=nnsum(ii)/float(kkk)
    mmsum(ii)=mmsum(ii)/float(kkk)
100 continue

       if(imin.ne.0) then
    do 110 ii=1,natoms
    ntype(ii)=ntype1(ii)
110 continue
       endif

    write(6,*)
   &     '-----------------------------------------------------'
    write(6,*) 'The least-energy configration is reached at'
    write(6,*)
   &     'the MC step = ',imin,', with total energy =',emin
    write(6,*)
   &     'Average energy over the last ',kkk,' steps =',eaver

    call statistics(neighh,ntype1,natoms,n,nnsa,mma)

    write(6,*)
   &'-----------------------------------------------------'
    write(6,120) kkk
120 format(' Statistics',7x,'Before',10x,'Minimum-energy case'
   &       ,3x,'Average of',I6,' steps')
    write(6,121)
121 format(' COORD No',5x,3('Type 1',3x,'Type 2',7x)
   &       /' --------',5x,3('------   ------',7x))
    if(imin.eq.0) then
    write(6,130) (j,nnsp(j),mmp(j),nnsp(j),mmp(j),
   &                     nnsum(j),mmsum(j),j=6,n)
    else
    write(6,130) (j,nnsp(j),mmp(j),nnsa(j),mma(j),
   &                     nnsum(j),mmsum(j),j=6,n)
    endif
130 format(I5,I13,I9,I13,I9,I13,I9)

    ndisp1=nnsp(6)+nnsp(7)+nnsp(8)+nnsp(9)
    disp1=ndisp1/float(ndisp1+nnsp(12))
    ndisp2=mmp(6)+mmp(7)+mmp(8)+mmp(9)
    disp2=ndisp2/float(ndisp2+mmp(12))
    disp3=(ndisp1+ndisp2)/float(ndisp1+nnsp(12)+ndisp2+mmp(12))
    write(6,135) disp1,disp2,disp3

    ndisp1=nnsa(6)+nnsa(7)+nnsa(8)+nnsa(9)
    disp1=ndisp1/float(ndisp1+nnsa(12))
    ndisp2=mma(6)+mma(7)+mma(8)+mma(9)
    disp2=ndisp2/float(ndisp2+mma(12))
    disp3=(ndisp1+ndisp2)/float(ndisp1+nnsa(12)+ndisp2+mma(12))
    write(6,135) disp1,disp2,disp3
```

```
  135 format(/'Types 1, 2 and Total Dispersions:',f7.4,f9.4,f13.4)
  160 call datetime(today2,now2)
      write(6,*) '-----------------------------'
      write(6,*) 'Finished Succuessfully'
      write(6,170) today2(2),today2(1),today2(3),now2
  170 format(2x,i2,'/',i2,'/',i4,'; time ',i2,':',i2,':',i2)
      write(6,*) '-----------------------------'
      write(6,*)
      return
      end

c-------------------------------------------------------------
      SUBROUTINE energy(ntype,na,neighh,coord,nn,a,b,c,wijz,etot)
c-------------------------------------------------------------
      IMPLICIT REAL*8(A-H,O-Z)
      dimension a(2),b(2),c(2),atom(3,na),coord(na,nn)
      dimension ntype(na),neighh(na)
      natoms=na
      n=nn
      etot=0.0d0
      do 10 i=1,natoms
      ntrand1=ntype(i)
      neigh1=neighh(i)
      e1=a(ntrand1)+b(ntrand1)*neigh1+c(ntrand1)*neigh1*neigh1
      etot=etot+e1
      do 10 j=1,neigh1
      ntrand2=ntype(int(coord(i,j)))
      neigh2=neighh(int(coord(i,j)))
      e2=a(ntrand2)+b(ntrand2)*neigh2+c(ntrand2)*neigh2*neigh2
      if(ntrand1.eq.ntrand2) wij=0
      if(ntrand1.ne.ntrand2) wij=wijz
      etot=etot+wij+e2
   10 continue
      etot=etot*0.5
      return
      end

c-----------------------------------------------------
      SUBROUTINE statistics(neighh,ntype,na,nn,nns,mm)
c-----------------------------------------------------
      IMPLICIT REAL*8(A-H,O-Z)
      dimension ntype(na),neighh(na),nns(nn),mm(nn)
      natoms=na
      n=nn
      do 10 j=1,n
      nns(j)=0
      mm(j)=0
   10 continue
      do 20 i=1,natoms
      do 20 j=1,n
      if(neighh(i).ne.j) go to 20
      if(ntype(i).eq.1) nns(j)=nns(j)+1
      if(ntype(i).eq.2) mm(j)=mm(j)+1
   20 continue
      return
```

```
    end
```

App.A.2. Input Data

```
5000000    500000       100   4990000
      0         2         0      2406
  800.0       3.0      0.10    -0.004
     Pt   -0.4015 -0.052320 0.0037590
     Pd    -0.17    -0.049     0.003

 NSTEPS     ISTEP     MSKIP    MSAVER
   ISFR      IDOM      NDOM    NATOMS
      T       TOL       PER      WIJZ
    at1        a1        b1        c1
    at2        a2        b2        c2

     Ni   -0.5530 -0.007794 0.0006268
     Cu   -0.3925 -0.001112 0.0008078
     Ag   -0.2397  -0.01601  0.001301
     Au   -0.3049  -0.02587  0.002070
     Pt   -0.4015  -0.05232  0.003759
     Pd    -0.17    -0.049     0.003

  WIJ/Z   Au-Pt               0.0226
  WIJ/Z   Cu-Pt              -0.0336
  WIJ/Z   Ag-Pt               0.0000
  WIJ/Z   Pd-Pt               -0.004
```